SpyCombinator Assembly of Bispecific Binders

Claudia L. Driscoll[1,2], Anthony H. Keeble[1,2], and Mark Howarth[1,2]*

[1]Department of Biochemistry, University of Oxford, South Parks Road, Oxford, OX1 3QU, UK.
[2]Department of Pharmacology, University of Cambridge, Tennis Court Road, Cambridge, CB2 1PD, UK.

*Corresponding author and Lead Contact:
Mark Howarth,
Department of Pharmacology,
University of Cambridge,
Tennis Court Road,
Cambridge,
CB2 1PD,
UK
E-mail: mh2186@cam.ac.uk

Keywords: chemical biology, uncaging, immunotherapy, bifunctional, tyrosine kinase

ABSTRACT

Bispecific antibodies are a successful and expanding therapeutic class, bridging two cell-types or engaging two different molecules on the same cell. Bispecifics unlock avenues towards synergy, resistance evasion, and signaling bias. Standard approaches to generate bispecifics are complicated by the need for disulfide reduction/oxidation or cloning of each binder molecule in two different formats. Here we present a modular approach to bispecifics using SpyTag/SpyCatcher spontaneous amidation, where all binders are cloned in the same format, bearing a SpyTag. Two SpyTag-fused antigen-binding modules can be precisely conjugated onto DoubleCatcher, a tandem SpyCatcher where the second Catcher is unreactive until unveiling of reactivity using site-specific protease. Assembly on DoubleCatcher is efficient in phosphate-buffered saline at 37 °C, with half-times less than 5 min for both SpyCatcher arms and over 97% bispecific homogeneity. We engineer a panel of DoubleCatchers, locked through disulfide bonds to direct binders to project in different directions from the hub. We establish a generalized methodology for one-pot assembly and purification of bispecifics in 96-well plate format. A panel of Fab, affibody or nanobody binders recognizing different sites on HER2 were coupled to DoubleCatcher, revealing unexpected combinations with anti-proliferative or pro-proliferative activity on HER2-addicted cancer cells. Bispecific activity depended sensitively on both the order of the binders within the assembly and the geometry of DoubleCatcher scaffolds. These findings support the need for straightforward assembly in different formats. SpyCombinator provides a simple and scalable tool to discover synergy in bispecific activity, through modulating receptor organization and geometry.

Introduction

Bispecific antibodies are biological matchmakers, bringing together two different target molecules or two different parts of the same target (Hofmann et al., 2020). Bispecifics have

had clinical success in cancer therapy by directing cytotoxic T cells to cancer-specific antigens (Hofmann et al., 2020). There are also approved bispecific therapeutics that bridge proteins on the surface of the same cell (Labrijn et al., 2019; Vijayaraghavan et al., 2020). Cell signaling often naturally depends on co-localization of particular ligands at the cell-surface (Batada et al., 2006). Synthetic control of such signaling has been successful using bifunctional small molecules (Zheng et al., 2022), DNA nanostructures (Shaw et al., 2014), and non-antibody protein-based binders (Mohan et al., 2019). The response of the cell is often exquisitely sensitive to the timing and spatial orientation of this bridging between surface targets (Moraga et al., 2015). Therefore, despite the numerous successes from bispecifics, there remains a huge range of unexplored combinations of bispecifics that could illuminate the principles of cell signaling and provide valuable therapeutic leads. It is an exciting challenge in protein engineering to facilitate the screening of bispecific combinations.

The most common routes to generate bispecifics depend upon rearrangement of IgG architecture, particularly through knob-into-hole generation of heterodimeric Fc domains (Spiess et al., 2013), or disulfide bond shuffling in the Fabs (Dengl et al., 2020; Labrijn et al., 2013). Alternative bispecific pairing has been achieved by conjugating the two binders using sortase (Andres et al., 2020), transglutaminase (Plagmann et al., 2009), click chemistry (Szijj and Chudasama, 2021) or split inteins (Han et al., 2017). However, these routes require each binder to be fused to the respective conjugation domain, such that each binder must be re-cloned, re-expressed, and re-purified in two formats to explore all possible bispecific combinations. Such a requirement is a major problem as the field moves towards exploring thousands of binders across the proteome (Cao et al., 2022; Colwill et al., 2011; Dübel et al., 2010).

Our group previously developed an efficient way to ligate genetically-encoded building blocks, through spontaneous isopeptide bond formation between a peptide Tag and a complementary Catcher protein (Keeble and Howarth, 2020; Keeble et al., 2022). SpyTag/SpyCatcher has been widely used for modular assembly of binders, enzymes and vaccines (Keeble and Howarth, 2020; Pardee et al., 2014). SpyTag003/SpyCatcher003 is a pair that we subsequently developed for reaction at a rate close to the diffusion limit, which maintains compatibility with all previous Spy versions (Keeble et al., 2019). SpyTag/SpyCatcher has been previously employed for bispecific assembly but faces the above limitation of having to clone each binder in two different formats, with one version fused to SpyTag and the other version fused to SpyCatcher (Chen et al., 2022; Keeble et al., 2022; Sutherland et al., 2019). In this work we establish a protease-activatable SpyCatcher003, to enable the generation of bispecific combinations where each binder only needs to be cloned into one common format – the SpyCombinator strategy. We show that binders can be assembled onto a panel of scaffolds, in order for the binders to project in different directions and change the orientation of the target receptor. We evaluate the SpyCombinator system against human epidermal growth factor receptor 2 (HER2), which has a central role in breast, gastric, and ovarian cancers through proliferative and anti-apoptotic signaling (Scholl et al., 2001). Employing SpyCombinator on a panel of 9 binders (affibody, nanobody or antibodies) allowed simple generation of 81 binder pairs against HER2 (9 with bivalent and 72 with bispecific binding activity). In order to demonstrate the mutability of our modular bispecific assembly approach, DoubleCatcher scaffolds that vary in dimensional architecture and rigidity were designed by modifying the linker separating Catcher domains, or by introducing an intramolecular disulfide bond. Again, SpyCombinator was applied to dimerize a subset of 9 pairs of anti-HER2 binders using the panel of 7 DoubleCatcher variants, to generate 63 bivalent binders spanning a diverse format space. These pairs of binders show major differences in their effect on cell survival and division, illustrating the potential of the SpyCombinator approach to accelerate combinatorial discovery and fine-tune cellular responses to designed receptor modulators.

Results

Masked SpyCatcher003 is a protease-activatable variant of SpyCatcher003

Our approach uses a tandem SpyCatcher003 for specific irreversible heterodimerization of any two antigen-binding units fused to SpyTag or its variants (i.e. SpyTag002 or SpyTag003) (Fig. 1A). The N-terminal SpyCatcher003 is accessible for reaction. The C-terminal SpyCatcher003 is masked. The non-reactive SpyTag003 D117A (SpyTag003DA) mutant (Keeble et al., 2019) is fused to the C-terminus of the second SpyCatcher003 via a flexible linker containing a tobacco etch virus (TEV) protease cleavage site (ENLYFQ/G) (Fig. 1A). Before cleavage, SpyTag003DA should bind tightly to SpyCatcher003, with K_d = 21 nM for the non-linked pair (Keeble et al., 2019), thus masking the reactive Lys of SpyCatcher003. The intramolecular SpyCatcher003/SpyTag003DA interaction should be entropically favored over a competing intermolecular interaction with SpyTag003 in solution. Following cleavage at the TEV site, the SpyTag003DA peptide will be free to dissociate, unmasking the reactive Lys of SpyCatcher003 to enable reaction with a second supplied SpyTag-linked binder. We performed all cleavages with superTEV protease, because of its efficient activity without the need for reductant (Cabrita et al., 2007).

We piloted the SpyCombinator strategy on a single SpyCatcher003 moiety. Masked SpyCatcher003 was cleaved with superTEV protease and incubated with a model fusion protein of SpyTag003 linked to maltose-binding protein (MBP) (Fig. 1B). This reaction proceeded efficiently to > 99% completion, with a half-life of reaction ($t_{1/2}$) of 2.7 ± 0.7 min (Fig. 1B, C, D). To reduce the extent to which SpyTag003DA dissociation limits the rate of reaction between TEV-cleaved Masked SpyCatcher003 with SpyTag003-MBP, the reaction temperature was elevated to 37 °C and the molar excess of SpyTag003-MBP relative to Masked SpyCatcher003 was increased to 5-fold. The muted reactivity of Masked SpyCatcher003 before cleavage was probed by incubating equimolar amounts of the construct with SpyTag003-MBP and monitoring the disappearance of Masked SpyCatcher003 over time by SDS-PAGE and densitometry (Fig. 1D, E). Under these conditions, we observed 3.7% reaction of Masked SpyCatcher003 with SpyTag003-MBP after 60 min, supporting effective silencing of SpyCatcher003 reactivity.

Establishing DoubleCatcher as a tool for controlled combination of distinct proteins

To design a platform that facilitates the conjugation of two Tagged proteins, Masked SpyCatcher003 was genetically fused to the C-terminus of a native SpyCatcher003 protein via a flexible Gly/Ser linker, to give DoubleCatcher (Fig. 2A, with sequence shown in Supplementary Fig. 1). The reactivity of each SpyCatcher003 moiety within the DoubleCatcher construct was determined by monitoring the reaction of DoubleCatcher with SpyTag003-linked model proteins before and after cleavage by MBP-superTEV protease. First, DoubleCatcher was incubated with 2-fold excess of SpyTag003 linked to the green fluorescent protein mClover3 in the absence of TEV protease (Fig. 2A, B). 91% reactivity of the N-terminal SpyCatcher003 was observed after 1 h, with a $t_{1/2}$ of 0.58 ± 0.05 min (Fig. 2C).

Next we incubated DoubleCatcher with two-fold excess SpyTag003-MBP for 2 h to saturate the N-terminal SpyCatcher003 moiety. Unreacted SpyTag003-MBP was removed from the reaction mixture by overnight incubation with bead-immobilized SpyCatcher003. Addition of superTEV protease to the crude mixture (4 h, 34 °C) induced cleavage of the SpyTag003DA mask from the C-terminal SpyCatcher003 (Fig. 2D). 2 µM of the cleaved construct was then reacted with a 5-fold molar excess of SpyTagged Small Ubiquitin-like Modifier (SUMO-SpyTag003) and the reaction was monitored over time, by SDS-PAGE and densitometry (Fig. 2E, F). Reaction to fill the second site of DoubleCatcher was rapid with $t_{1/2}$

of 3.6 ± 0.7 min, showing that the cleaved SpyTag003DA can be efficiently replaced by a reactive Tag.

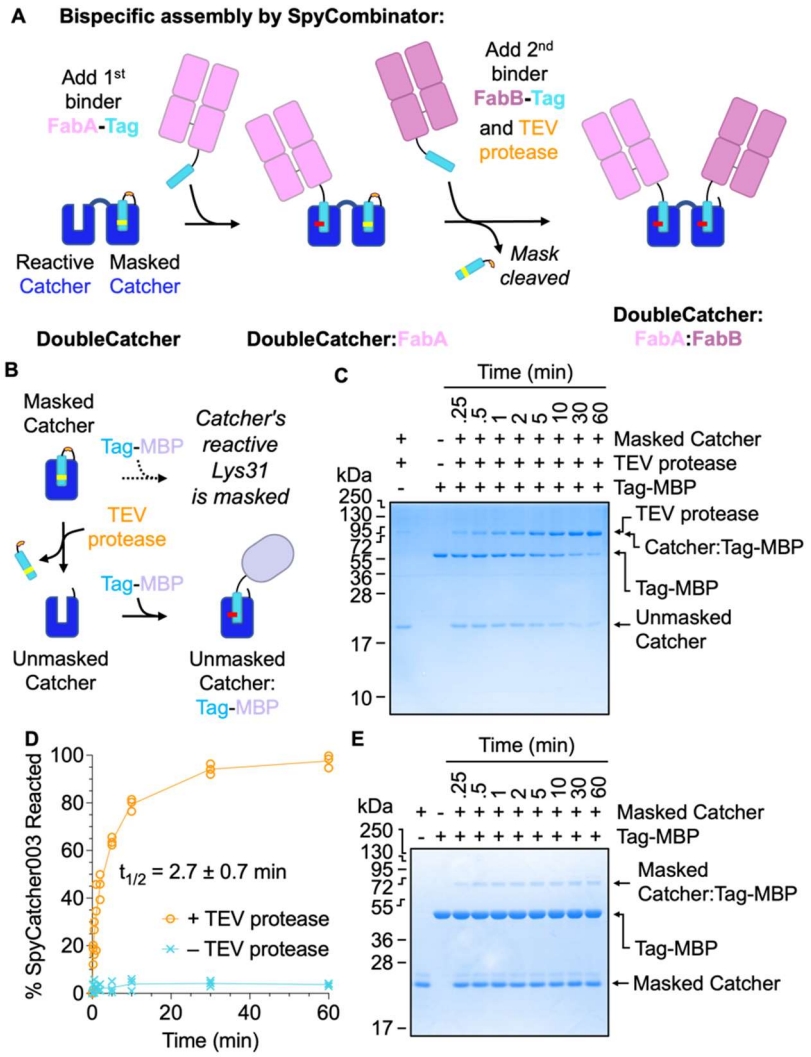

Figure 1. Masked SpyCatcher003 has protease-activatable reactivity. (**A**) SpyCombinator approach. DoubleCatcher consists of an accessible N-terminal SpyCatcher and a C-terminal SpyCatcher masked by the unreactive SpyTag003DA peptide. The first SpyTag-linked binder reacts with the N-terminal Catcher but is blocked from reacting at the second Catcher by the tethered unreactive SpyTag003DA peptide. Addition of TEV protease induces cleavage of SpyTag003DA, so that the second Catcher can be loaded with a different SpyTag-linked binder. SpyTag003 in cyan with D117A indicated in yellow, TEV protease site in orange, Fabs in pink, and isopeptide bond in red. A colon indicates covalently linked products. (**B**) Cartoon following protease-controlled unmasking of SpyCatcher003. Incubation of Masked Catcher with TEV protease enables cleavage and dissociation of SpyTag003DA from SpyCatcher003, allowing SpyTag003-linked proteins to react with SpyCatcher003 ('Unmasked Catcher'). (**C**) Efficient coupling after TEV protease unmasking. After incubation of Masked Catcher with TEV protease, the unmasked Catcher (5 µM) is incubated with equimolar SpyTag003-MBP for the indicated time, before SDS-PAGE with Coomassie staining. (**D**) Quantification of SpyCatcher003 reactivity with or without masking (individual replicates with means connected, n = 3), indicating the mean half-time of reaction, $t_{1/2}$. (**E**) Minimal reactivity of Masked SpyCatcher003 prior to TEV protease cleavage. Masked SpyCatcher003 was incubated with SpyTag003-MBP (both partners at 5 µM) for the indicated time at 37 °C, before SDS-PAGE/Coomassie.

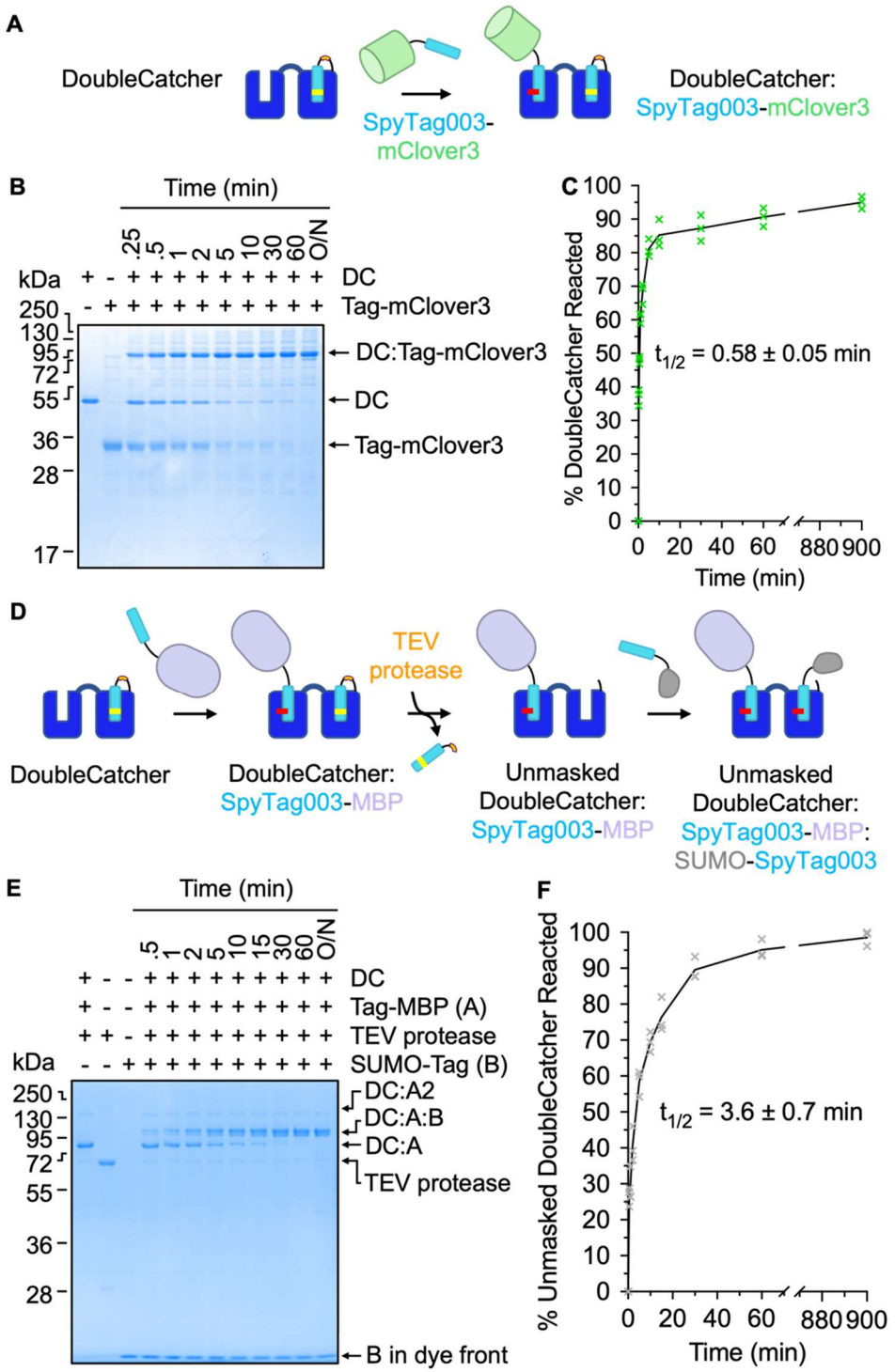

Figure 2. Dual conjugation of Tagged proteins to DoubleCatcher is fast and site-specific. (**A**) Schematic of covalent conjugation of SpyTag003-mClover3 to the reactive N-terminal Catcher of DoubleCatcher. (**B**) Time-course of reaction between DoubleCatcher (DC; 2.5 µM) and SpyTag003-mClover3 (5 µM), analyzed by SDS-PAGE/Coomassie. (**C**) Depletion of unreacted DoubleCatcher over the course of reaction was quantified by densitometry, following (B). (**D**) Schematic depicting unmasking and conjugation of the C-terminal Catcher of DoubleCatcher. (**E**) Reaction at the unmasked Catcher of DoubleCatcher. Following saturation of the N-terminal Catcher of DoubleCatcher with SpyTag003-MBP ('A'), the sample was incubated with TEV protease for 2 h at 34 °C. The resulting unmasked DoubleCatcher:SpyTag003-MBP (2 µM) was then reacted with SUMO-SpyTag003 ('B', 10 µM) over the time indicated, before SDS-PAGE/Coomassie. (**F**) Quantification of reaction at the unmasked Catcher of DoubleCatcher, based on (E). All triplicate data points are shown, with the line connecting the mean.

184 **Establishment of scalable heterodimerization of proteins using SpyCombinator**
185 A universal bispecific assembly platform for high-throughput screening requires a simple and
186 scalable methodology. In particular, procedures involving multiple rounds of column
187 chromatography will provide a bottleneck to the combinatorial complexity of bispecifics that
188 can be interrogated. Therefore, we next sought to optimize a one-pot reaction in which any two
189 Tagged binders can be conjugated to DoubleCatcher (Fig. 3A), and the resulting bispecific
190 molecule can be purified (Fig. 3B). For optimization, model ligands were assembled onto
191 DoubleCatcher: these were a SpyTag construct linked to three tandemly-repeated affibodies
192 against HER2 (SpyTag-AfiiHER2$_3$, ligand A) and SpyTag003 linked to a high stability MBP
193 tandem fusion ((MBP$_X$)$_2$-SpyTag003, ligand B) (Veggiani et al., 2016). These ligands lack free
194 Cys (avoiding impurity from inter-ligand disulfides) and have a difference in mass that permits
195 unambiguous detection of reactant and product bands by SDS-PAGE (Fig. 3A). The intact
196 masses of these purified reactants in PBS pH 7.4 were validated by electrospray-ionization
197 mass spectrometry (Supplementary Fig. 2).
198 In step 1 of our one-pot assembly route, DoubleCatcher reacts with a small molar excess
199 (1.25-fold) of SpyTag-AffiHER2$_3$, to ensure negligible unreacted DoubleCatcher in solution
200 (Fig. 3A). SDS-PAGE revealed 97% of the reaction contained the desired singly-occupied
201 DoubleCatcher:SpyTag-AffiHER2$_3$ species (Fig. 3C, lane DC + A). As observed for Masked
202 SpyCatcher003 reactivity tests (Fig. 1D), 3% contained DoubleCatcher conjugated to two
203 SpyTag-AffiHER2$_3$ molecules (Fig. 3C). To confirm where the homodimeric
204 DoubleCatcher:(SpyTag-AffiHER2$_3$)2 would run, we added superTEV protease (1/12th molar
205 equivalent) to the crude mixture; the homodimer in the reaction mixture increased to 30% ('DC
206 + A + TEV' lane in Fig. 3C). The identity of this by-product was corroborated by the increase
207 in the density of the band corresponding to AffiHER2$_3$ homodimer in a control reaction
208 containing twice the concentration of SpyTag003-AffiHER2$_3$ ('DC + A + TEV + A' lane in
209 Fig. 3C).
210 For subsequent unmasking and saturation of the C-terminal SpyCatcher003 moiety,
211 superTEV protease (1/12th molar equivalent) and (MBP$_X$)$_2$-SpyTag003 (5-fold molar excess,
212 'B') were added simultaneously to the singly saturated DoubleCatcher (*Step 2*, Fig. 3A). Thus,
213 immediately upon cleavage of SpyTag003DA, the concentration of (MBP$_X$)$_2$-SpyTag003 in
214 solution should be 20 times that of unreacted SpyTag-AffiHER2$_3$ and so homodimer formation
215 is minimized. Indeed, AffiHER2$_3$ homodimer accounted for only 3% of the total species in the
216 reaction mixture ('DC + A + TEV + B' in Fig. 3C). Trace (3%) formation of DoubleCatcher
217 conjugated to two (MBP$_X$)$_2$-SpyTag003 molecules ('MBP homodimer') was observed by SDS-
218 PAGE, validated by the formation of a band of equivalent mobility in a reaction with
219 DoubleCatcher, superTEV protease and (MBP$_X$)$_2$-SpyTag003 alone ('DC + B + TEV + B' lane
220 in Fig. 3C).
221 For depletion of excess SpyTag- or SpyTag003-linked binder from the desired product,
222 the crude reaction mixture was incubated with bead-immobilized SpyCatcher003, by adding
223 beads in a 1:1 suspension with PBS directly to the reaction mixture (*Step 3*, Fig. 3A and Fig.
224 3B). The purity of DoubleCatcher:SpyTag-AffiHER2$_3$:(MBP$_X$)$_2$-SpyTag003 following
225 purification was assessed by SDS-PAGE densitometry as 95% (excluding superTEV protease)
226 (Purification lane in Fig. 3C). Based on SDS-PAGE, superTEV protease (70 kDa, Fig. 3D, E)
227 was the major contaminant. Since TEV protease has exceptional specificity for its target
228 sequence, which is not found in the human proteome, and has been expressed before without
229 effect on cells (Gray et al., 2010), we did not consider it necessary to remove. However, it
230 should also be possible to add amylose-agarose to the well, for depletion of the MBP-linked
231 superTEV protease, if considered helpful.
232 We also validated the bispecific assembly by mass photometry, allowing single
233 molecule-based assessment of each species in solution (Asor and Kukura, 2022). The peak

corresponding to DoubleCatcher:SpyTag-AffiHER2$_3$:(MBP$_X$)$_2$-SpyTag003 was observed with a mass of 144 kDa, matching well to the 144.6 kDa predicted mass (Fig. 3D). The second peak of 70 kDa, fitted well to MBP-superTEV protease (Fig. 3D), as validated by running MBP-superTEV protease on its own (Fig. 3E).

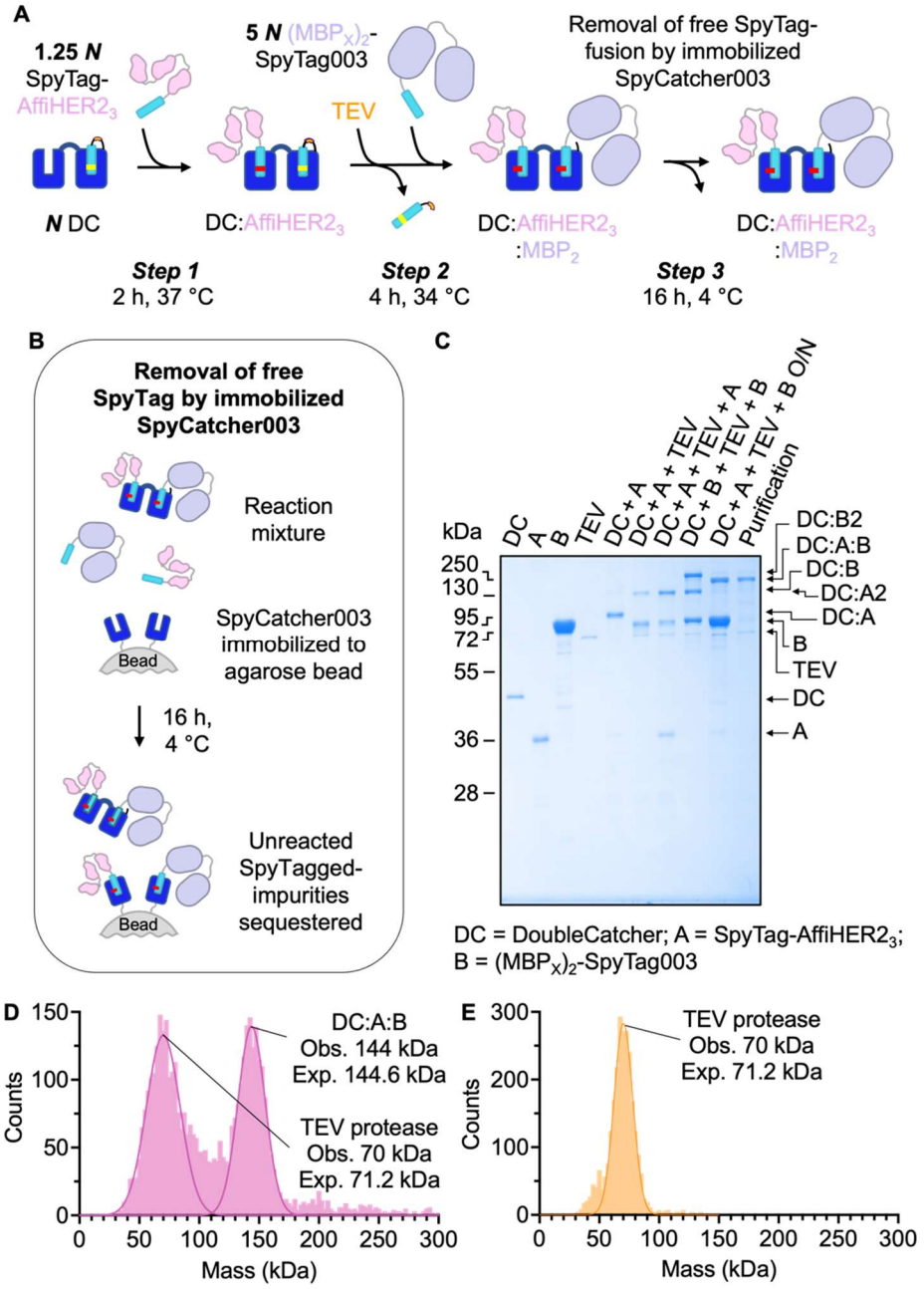

Figure 3. One-pot conjugation of DoubleCatcher with Tagged model proteins to yield a bispecific with high purity. (**A**) Schematic depicting assembly of SpyTag-AffiHER2$_3$ (pink) and (MBP$_X$)$_2$-SpyTag003 (purple) onto DoubleCatcher (DC, blue). ***N*** represents the concentration of DoubleCatcher and then the relative molarity of each Tag-binder is marked. Immobilized SpyCatcher003 removes free Tagged proteins, leaving the bispecific in solution. (**B**) One-pot bispecific assembly as in (A), monitored by SDS-PAGE/Coomassie. (**C**) Schematic of purification of excess Tag-fusion by immobilized SpyCatcher003 S49C in Step 3. (**D**) Mass photometry of SpyCombinator reaction. Peaks are shown for the product of coupling, as in (B), with observed and expected M_w indicated, confirming the identity of the target bispecific. The other species in the reaction was TEV protease. (**E**) Mass photometry of TEV protease alone, annotated as in (D).

Anti-HER2 bispecifics assembled by SpyCombinator induce various anti-proliferative or proliferative effects in HER2-addicted cancer cells

The work presented above demonstrates the efficient assembly of bispecific ligands through DoubleCatcher. We then aimed to complement the SpyCombinator platform with a screening approach of equal throughput on binders against the important cell-surface target of HER2. The relative activity of each signaling pathway and downstream physiological outcome has been attributed to different ligands stabilizing receptor dimers in distinct conformations, inducing distinct phosphorylation of the 17 sites in HER2's intracellular domain (Freed et al., 2017). Although the functional selectivity of native Receptor Tyrosine Kinase ligands has been extensively studied, this bias is yet to be exploited for personalized cancer therapies. Thus, we sought to assemble a large matrix of anti-HER2 bispecifics which differ in format and screen for their ability to alter HER2 activity (Brack et al., 2014; Stüber et al., 2021). Binders specific to each subdomain of the HER2 extracellular region were identified (Fig. 4A, B), including Fabs based on the clinically used Pertuzumab ('Pert') and Trastuzumab ('Tras', known commercially as Herceptin). Tras is a Trastuzumab variant with a point mutation to enhance binding stability (Jain et al., 2013). Each binder was expressed as a SpyTag003-fusion in Expi293F cells, except the nanobody (nanoHER2) (Verheije et al., 2013) and affibody (AffiHER2) (Feldwisch et al., 2010) which were expressed in *E. coli*. We confirmed the identity of each binder using electrospray-ionization mass spectrometry (Supplementary Fig. 3). Fusions to SpyTag are conventionally expressed with a spacer to favor high reactivity with SpyCatcher and optimal activity of the fused domain (Keeble and Howarth, 2019). We expressed a variant of Tras with no linker to SpyTag003, to test the importance of linker flexibility on activity, termed Tras NoLink. The NoLink variant was confirmed to react to 97% in 60 min in PBS pH 7.4 at 37 °C with DoubleCatcher, an efficiency comparable to the linker-containing parental construct (99% in 60 min under equivalent reaction conditions; Supplementary Fig. 4), confirming that reactivity is not impaired by removing the linker between the Fab and the reactive peptide. Each binder was dimerized with itself or another binder using SpyCombinator methodology (Fig. 3A). We studied the effects of the resulting matrix of anti-HER2 bispecifics and homodimers on metabolic activity in HER2-addicted BT474 cells (a human ductal breast carcinoma cell-line) or SKBR3 cells (a human adenocarcinoma cell-line), quantifying using the resazurin assay (Stüber et al., 2021).

Following incubation of BT474 or SKBR3 cells with anti-HER2 bispecific assemblies (100 nM) for 96 h, the change in metabolic activity was calculated relative to untreated cells (Fig. 4C, D). We discovered that the different assemblies exhibited a range of antagonistic and agonistic activities. We found that bispecific constructs displaying one or more arm binding to domain II (39S, HFS2, or Pert) are consistently anti-proliferative.

Anti-HER2 bispecifics also showed different potencies in SKBR3 cells relative to BT474 cells. Firstly, a higher number of bispecifics had significant proliferative activity in BT474 (20 constructs) than in SKBR3 (10 constructs). Secondly, constructs with significant anti-proliferative activity were more potent in BT474 (average metabolic activity of significant antagonists = 58.4 ± 20.4%) than in SKBR3 (average metabolic activity of significant antagonists = 64.2 ± 7.0%). In BT474 cells, the potent antagonist Tras NoLink-Tras (74.1 ± 6% (BT474) metabolic activity after 96 h treatment) showed no activity when assembled in the opposite orientation: Tras-Tras NoLink (103 ± 1% for BT474 metabolic activity). Importantly, the same orientation-dependence was observed in SKBR3 cells for the significantly active bispecifics nanoHER2-HFS2, Tras-AffiHER2, nanoHER2-AffiHER2, MF3958-Tras NoLink, Tras-39S, 39-Tras NoLink, Tras-MF3958; where assembly of these binders in the opposite orientation removes their significant agonistic or antagonistic activity.

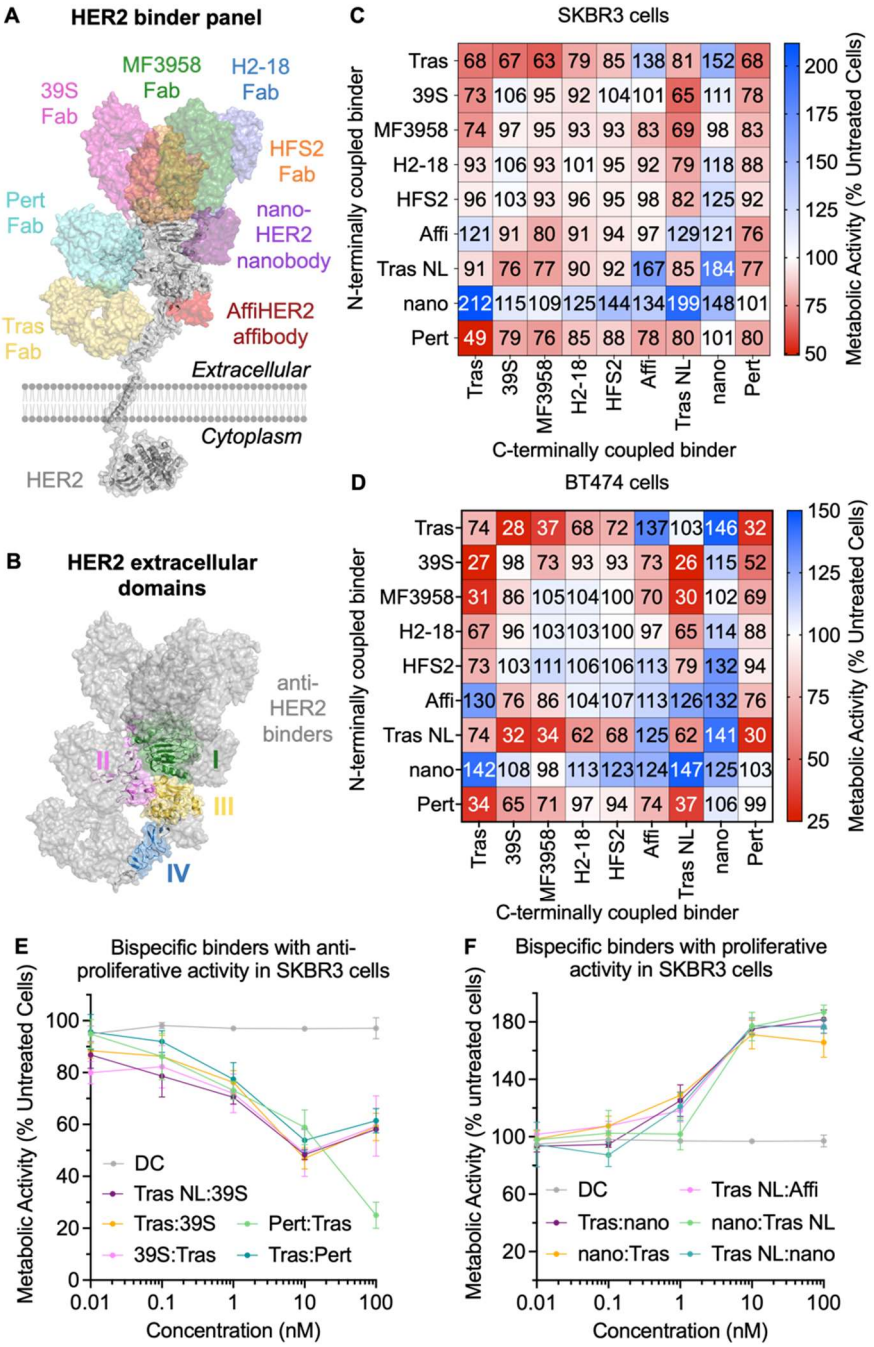

Figure 4. SpyCombinator bispecific panel exhibits a range of pro- or anti-proliferative activities on cancer cells. (**A**) Binding sites on HER2 for the panel of anti-HER2 binders. For each subdomain (I-IV) of HER2's extracellular domain at least one binding molecule was identified and the cartoon illustrates their binding site on HER2 (gray), with each binder in a different color. (**B**) Subdomains of HER2's extracellular domain are colored, with anti-HER2 binders from (A) overlaid in gray. (**C**) SpyCombinator anti-HER2 panel effect on SKBR3 cell proliferation. The vertical column indicates the binder at the N-terminal site of DoubleCatcher. The horizontal column shows the binder at the C-terminal site of DoubleCatcher. The effect on proliferation of SKBR3 cells with 100 nM bispecific after 4 days from resazurin assay is shown as a heat map, with red showing reduced proliferation and blue showing enhanced proliferation, compared to the DoubleCatcher alone control at 100%. (**D**) Bispecific panel effect on proliferation of BT474, as in (B). (**E**) Titration curves for the top 5 bispecifics with significant anti-proliferative activity in SKBR3 cells, assayed as in (C). (**F**) Titration curves for the top 5 bispecifics with significant pro-proliferative activity in SKBR3 cells, assayed as in (C).

313 Examining the effect of removing the linker between binder and SpyTag003, the average
314 difference between bispecifics with at least one Fab0.11 versus at least one Tras NoLink was
315 only 2%. The similarity between the activities of Tras and Tras NoLink supports the usage of
316 linker-free binder-SpyTag fusions in future screens, where it will be beneficial to maximize
317 rigidity in the bispecific molecule and impart control over target geometries. Together, these
318 results highlight the importance of screening epitope-diverse bispecific binders in multiple
319 formats and orientations.
320
321 **DoubleCatcher architecture can be customized**
322 As with most bispecific antibodies, the format of a bispecific binder built using SpyCombinator
323 may be influenced by the identity of the SpyTag003-linked binder, and by the order in which
324 the binders are coupled. However, the overall shape, size, and flexibility of the bispecific
325 molecule may also be determined by the DoubleCatcher module itself. To amplify the format
326 space to be screened, matrices of bispecific antibodies could therefore be developed in three
327 dimensions: varying two binder arms against the targets of interest and, in parallel, varying the
328 DoubleCatcher module. The highest-scoring AlphaFold2-predicted structure for
329 DoubleCatcher is displayed in Fig. 5A (left), with the position and orientation (N to C) of the
330 two SpyTag binding sites represented by cyan vectors. Modifications to the DoubleCatcher
331 architecture that change the relative spacing and orientation of the cyan vectors will reflect
332 changes in the structural relationship between the two target-binding arms in the final
333 bispecific.
334 Modifications to the architecture of DoubleCatcher may be achieved by varying the
335 linker connecting the two SpyCatcher003 moieties. The amenability of DoubleCatcher to
336 linker modification was tested by substituting the Gly/Ser linker with the central helix from the
337 *Bacillus stearothermophilus* ribosomal protein L9 (Kuhlman et al., 1997). The DoubleCatcher
338 variant with the helical linker is termed 'DoubleCatcher H-lock' (Fig. 5A, right, and sequence
339 in Supplementary Fig. 1). Size-exclusion chromatography analysis of Ni-NTA-purified
340 DoubleCatcher H-lock revealed its apparent molecular mass was 17 kDa larger than
341 DoubleCatcher (Fig. 5D, E), while the predicted increase in mass is only 3.5 kDa, as validated
342 by electrospray-ionization mass spectrometry (Supplementary Fig. 2).
343 One approach to increasing the rigidity of the DoubleCatcher module that overcomes
344 the flexibility of the SpyCatcher003 termini is to engineer a covalent linkage between the two
345 Catcher domains. A pair of residues (one residue from each SpyCatcher003) that reside in loop
346 regions and close proximity (1.2 nm) within each of the the five highest-confidence predicted
347 structures of DoubleCatcher was chosen as the site for cysteine substitution to engineer a
348 SpyCatcher003-SpyCatcher003 intramolecular disulfide bond. The AlphaFold2-predicted
349 structure of the double-cysteine variant designed from the top-predicted DoubleCatcher
350 structure is presented in Fig. 5B and is termed 'DoubleCatcher α-lock'. The substantially less
351 variable average distance between Nε of the reactive Lys residues of each SpyCatcher003 in
352 the top 5 AlphaFold2-predicted structures of DoubleCatcher α-lock (4.7 ± 0.04 nm) suggests
353 the two SpyCatcher003s may have low relative mobility. The DoubleCatcher double-cysteine
354 variants designed from the four remaining predicted structures of DoubleCatcher are presented
355 in Fig. 5C. Therefore, the combination of SpyTagged antigen binders using these
356 DoubleCatcher variants should provide conformationally distinct bispecific binders that bind
357 targets in different orientations.
358 Size-exclusion chromatography profiles of Ni-NTA-purified double-cysteine DoubleCatcher
359 variants reveal that the construct exists as two species: one main peak corresponding to
360 monomer and one minor peak that corresponds to covalent dimer (Fig. 5D).
361

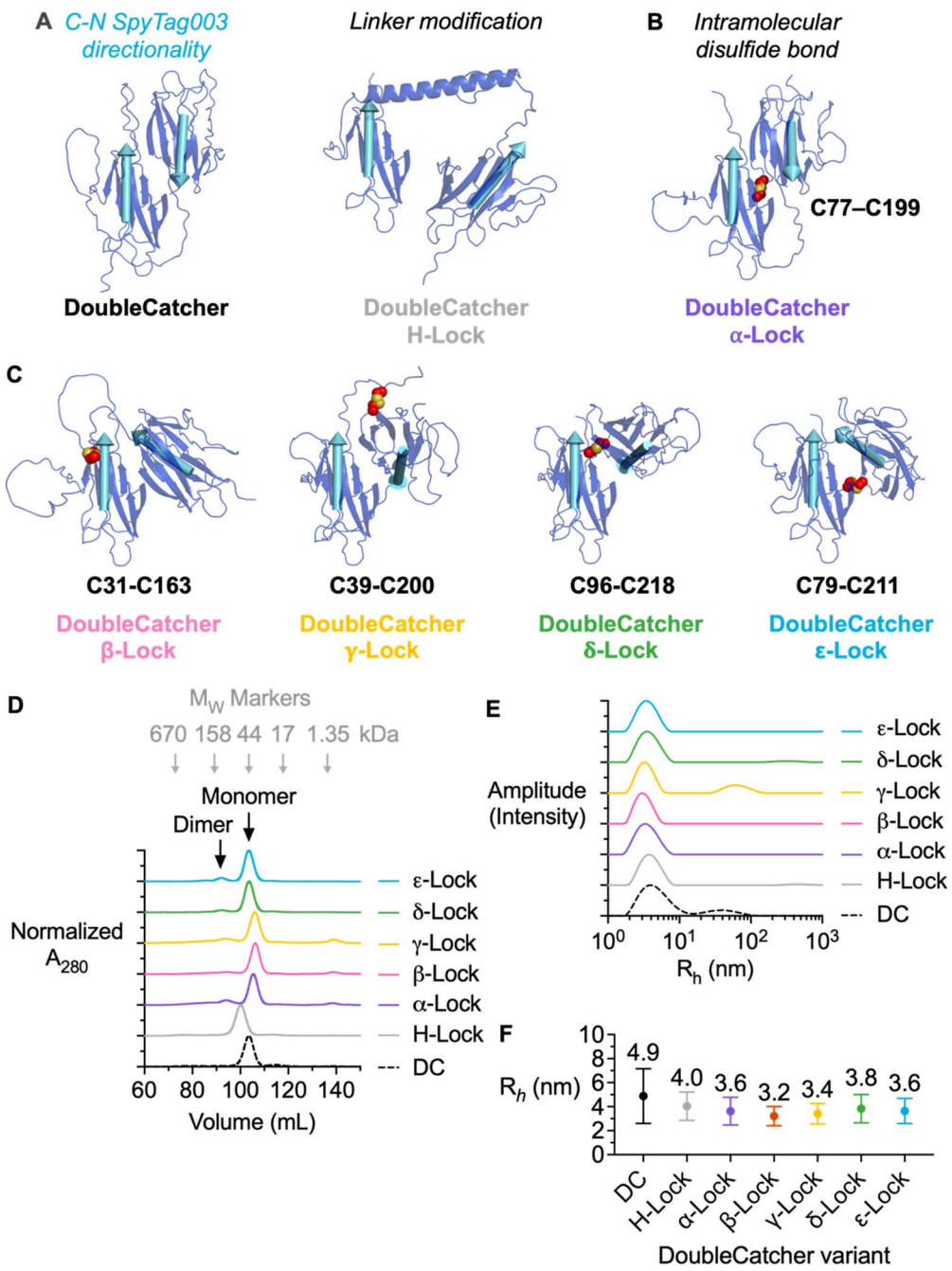

Figure 5. Panel of DoubleCatcher architectures. (**A**) Schematic of DoubleCatcher or DoubleCatcher with helical spacer. AlphaFold2-predicted structures show DoubleCatcher dark blue and the Tag as a cyan vector, indicating the direction that a Fab-SpyTag fusion would project. The flexible linker in DoubleCatcher (left) was replaced with a stable α-helical linker in DoubleCatcher H-lock (right). (**B**) Schematic of DoubleCatcher locking through an engineered disulfide bond. AlphaFold2-predicted structure, as in (A). The residues selected for Cys substitution (left) and the disulfide bond in the resulting double-cysteine mutant (DoubleCatcher α-Lock) are labeled as red spheres with sulfur in yellow. (**C**) Schematic of the other DoubleCatcher Lock variants, labeled with their Cys substitutions. (**D**) Size-exclusion chromatography of DoubleCatcher variants normalized by A_{280}. Chromatograms are staggered by 1 from adjacent curves in the y-axis. The apparent molecular weights of each species were calculated following calibration with molecular weight standard proteins (Bio-Rad) (grey arrows). (**E**) Dynamic light scattering of DoubleCatcher variants in PBS. Traces are staggered by 1 from adjacent curves in the y-axis. (**F**) Quantification of dynamic light scattering, showing mean hydrodynamic radius (R_h) ± 1 s.d. (n = 10) for each DoubleCatcher.

DoubleCatcher double-cysteine monomer was incubated with $CuSO_4$ to drive disulfide bond formation prior to downstream analyses. The identity and disulfide bond formation of each DoubleCatcher was validated by electrospray-ionization mass spectrometry (Supplementary Fig. 2). The DoubleCatcher variants were analyzed by dynamic light scattering (DLS) (Fig. 5F), with quantification shown in Fig. 5G. As expected, both the mean hydrodynamic radius (R_h) and the mean s.d. of the double-cysteine mutants (3.5 ± 1.0 nm, mean ± 1 s.d., n = 10) were less than those for the cysteine-free variants (4.5 ± 1.7 nm, mean ± 1 s.d., n = 10), consistent with reduced flexibility within the architecture.

SpyCombinator-assembled anti-HER2 bispecific binders are sensitive to DoubleCatcher architecture

To investigate the sensitivity of HER2 signaling to dimer geometry, a small-scale matrix of anti-HER2 bispecific binders was assembled by using each of the 7 designed DoubleCatcher variants to dimerize Tras NoLink, nanoHER2, and AffiHER2 in all 9 possible permutations. The assembled bispecific binders were added to HER2-addicted SKBR3 cells (100 nM) for 96 h, after which the change in metabolic activity was calculated (Fig. 6A, B). For each pair of binders, cells were treated with a mixture of the purified binders (100 nM) without DoubleCatcher, to test for monovalent binder activity- 'No DC' matrix in Fig. 6A. Simultaneously, purified DoubleCatcher variants (100 nM) were added to cells, to test for any activity of scaffold alone (Fig. 6A).

In a similar way to the orientation-dependent activity of bispecifics assembled in Figure 4, we repeatedly found that the potency of specific combinations of binders were enhanced when assembled onto a different DoubleCatcher variant. The most pronounced example of this is for the pro-proliferative DoubleCatcher β-lock bispecifics containing nanoHER2: relative to the DoubleCatcher-assembled bispecifics, those assembled with DoubleCatcher β-Lock induced +25.6 % greater proliferation in SKBR3 cells. Similarly, the anti-proliferative activity of Tras NL-Tras NL (84.8 ± 6.8% metabolic activity for the DoubleCatcher-assembled bispecific) was enhanced when dimerized with DoubleCatcher H-Lock (75.9 ± 2.5%), DoubleCatcher α-Lock (79.5 ± 3.9%), DoubleCatcher γ-Lock (80.4 ± 3.4%), DoubleCatcher *δ*-Lock (73.6 ± 4.9%), and DoubleCatcher ε-Lock (72.5 ± 4.3%). In addition to increased potency, it was also observed that the ability of some pairs of binders to either agonize or antagonize HER2 signaling was switched when assembled into a different architecture. Specifically, the bispecific AffiHER2-Tras NoLink showed mild agonistic activity on the DoubleCatcher scaffold (112.5 ± 6.6% metabolic activity), yet the same bispecific assembled using DoubleCatcher H-Lock exhibited strong antagonistic activity under the same conditions (82.5 ± 11.1%). The same switch in activity was even more marked for Tras NoLink-AffiHER2 assembled in DoubleCatcher γ-Lock (78.6 ± 3.1 %) relative to DoubleCatcher (127.7 ± 4.1%), accentuating the value of screening multiple formats in the assembly of bispecifics.

Discussion

Here we have demonstrated SpyCombinator assembly, allowing controlled and precise construction of bispecific binders through sequential SpyTag/SpyCatcher conjugation. The SpyCombinator platform offers a plug-and-play approach in which the antigen-binding building blocks exist in a common format, fused to the commonly-employed SpyTag peptide or its subsequent generations (Keeble and Howarth, 2020; Keeble et al., 2019). Unlike standard approaches to bispecific assembly (Hofmann et al., 2020), SpyCombinator eliminates the need to clone and express each pair of binding proteins into more than one format. Neither SpyTag nor SpyCatcher require any cysteines and the overall assembly is ligated through amide bonds (Keeble and Howarth, 2020), so SpyCombinator avoids the careful optimization and instability that may arise from bispecific assembly relying on disulfide bond reduction and oxidation.

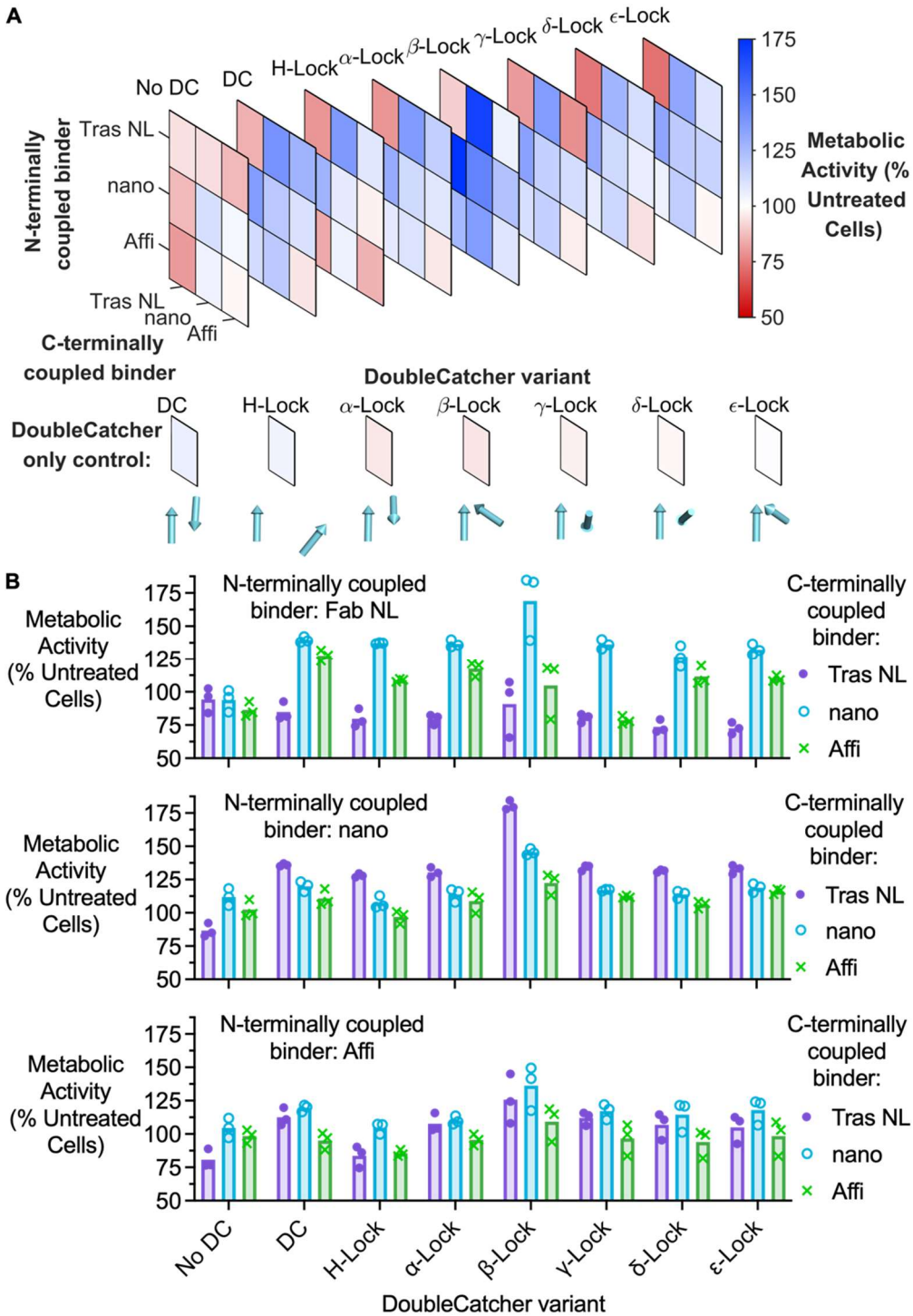

Figure 6. Architectural modifications to anti-HER2 bispecifics change the signaling effects. (**A**) Different DoubleCatcher scaffolds change HER2 signaling. Matrices of anti-HER2 bispecifics were assembled by SpyCombinator using distinct DoubleCatcher variants. Treatment of SKBR3 cells with the bispecifics (100 nM, 4 days) revealed DoubleCatcher-dependence on their pro- or anti-proliferative potency, as determined by resazurin assay. Mean metabolic activity, relative to untreated control, are presented as stacked heat maps, with red showing reduced proliferation and blue enhanced proliferation. Activity following 100 nM DoubleCatcher variant alone was measured in parallel. Below each variant, vectors depict the position and orientation of C-N SpyTag003-binding groove within each SpyCatcher003 moiety, such that the binder projects in the direction of the vector arrowhead. (**B**) Graphical representation of DoubleCatcher-dependence for cell proliferation, following (A). Each data-point is shown (n = 3), with the bar indicating the mean, ± 1 s.d..

Optimization of SpyCombinator conditions produced a generalized pipeline that generates bispecifics with up to 97% purity relative to homodimeric by-products. The modularity of the platform invites customization of each constituent, exemplified here through DoubleCatcher variants with different linkers or intramolecular disulfide bonds. There is potential in future work for substantial diversification of the DoubleCatcher module, to generate additional bispecific architectures (Baker, 2019).

In this study, anti-HER2 binders varying in epitope and size were permuted into a matrix of bispecifics. We identified anti-HER2 bispecifics with major differences in their pro- or anti-proliferative activity. Interestingly, this proliferative activity depended not only on the identity of the anti-HER2 monomers, but also on the order of coupling to DoubleCatcher, affirming the importance of screening paratope orientation (Scheer et al., 2012; Stüber et al., 2021). Furthermore, in assembling a small panel of anti-HER2 binders into bispecifics using DoubleCatchers of varying geometries and flexibilities, we found that the activity or potency of particular pairs of binders is dependent on their scaffold. Cellular effects of bispecific bridging depend upon an intricate balance of allosteric interactions between intracellular kinase domains (Zhang et al., 2006), altered heterodimer formation with other receptors (Gu et al., 2014), and receptor dynamics at the plasma membrane or endolysosomal compartments (Scheer et al., 2012; Stüber et al., 2021). Therefore, being able to screen large numbers of bispecific combinations in multiple formats is crucial to the discovery of the most potent effector activity. HER2 dimerization is facilitated predominantly by interactions between domain II residues (Arkhipov et al., 2013), so these bispecifics are likely to block HER2 dimerization and activation. Conversely, bispecifics harboring the small, non-domain II binders nanoHER2 (16 kDa) or AffiHER2 (15 kDa) display potent proliferative activity. Indeed, the bispecific constructs with significant agonistic activity in both SKBR3 and BT474 cells all comprised at least one of nanoHER2 or AffiHER2. Where agonistic activity of biparatopic anti-HER2 molecules has been observed, it has been suggested to result from favouring HER2 homodimerization over heterodimerization, or from a shorter distance between antigen-binding sites (Gu et al., 2014; Kast et al., 2021; Scheer et al., 2012). Considering their small size, DoubleCatchers coupled to either nanoHER2 or AffiHER2 may bridge HER2 molecules close enough for trans-phosphorylation by HER2 kinase domains. This result may be explained by the differential total expression of HER2, as well as the expression of Epidermal Growth Factor Receptor (EGFR) and HER3 relative to HER2. BT474 expresses HER2 to a greater extent (~2.8×10^6 copies per cell) (Kamashev et al., 2022) relative to SKBR3 (~1.2×10^6 copies) (Hendriks et al., 2013). Both express HER3 to a similar level (1-1.2×10^6 copies) but SKBR3 expresses ~3-fold more EGFR (2.2×10^5 copies) than BT474 (7×10^4 copies) (Brockhoff et al., 2001). HER2-HER3 dimerization mediates activation of PI3K/Akt and proliferation axis (Junttila et al., 2009), while HER2-EGFR dimers favor MAPK/ERK and pro-survival signaling (Kirouac et al., 2016). Therefore, for bispecifics preventing HER2 homodimerization but not occluding domain II of HER2 (for example, domain I-binding H2-18 or MF3958), heterodimerization may occurs more favorably. This could result in a higher frequency of proliferative HER2-HER3 dimers in BT474 than SKBR3.

Differences in activities of anti-HER2 bispecifics have been attributed to the architecture of the molecule, in addition to binder identity. Specifically, this includes the binder's ability to oligomerize HER2 monomers, resulting in arrested receptor diffusion compartmentalization into membrane nanodomains (Stüber et al., 2021); the binder-defined distance between cross-linked HER2 molecules (Kast et al., 2021); the distortion of HER2 extracellular domain upon binding, such that its ability to homo/hetero-dimerize is affected (Gu et al., 2014); and the amenability of the binder's format to increased bispecific-HER2 complex stoichiometries (Brack et al., 2014). Our DoubleCatcher panel introduces variation in

relative paratope orientation, distance between paratopes, and scaffold rigidity. We hypothesize that these parameters and their combinations each influence HER2 dynamics by one or more of the mechanisms highlighted. However, further experiments are required to decipher their biochemical behaviours, such as employing BRET to study homo- vs. hetero-dimer formation (Siddiqui et al., 2013), single-particle tracking analysis to quantify changes in receptor diffusion kinetics (Freed et al., 2017), or nanoparticle-aided cryo-electron microscopy to gain insight into the conformational homogeneity, and thus rigidity, of different SpyCombinator-assembled bispecific molecules (Ki et al., 2021).

Control over Tag/Catcher activity has previously been achieved using pH (Vester et al., 2022), redox (Matsunaga et al., 2013; Wu et al., 2018), temperature (Cao et al., 2017), or light (Hartzell et al., 2021; Ruskowitz et al., 2023). While these switches have an array of valuable applications, the simple generation and large change in reactivity of the protease-uncaging system is advantageous for bispecific assembly. In particular, redox changes on the Catcher would be undesirable for assembling building blocks that themselves contain disulfides, notably nanobodies and various peptide hormones. A potential limitation of SpyCombinator is that SpyTag/SpyCatcher is derived from *Streptococcus pyogenes*, so immunogenicity may affect the use of DoubleCatcher bispecifics as clinical candidates (Rahikainen et al., 2021). Nonetheless, Catcher bispecifics can be important leads to inform the design of biologics and identify novel targets/epitopes for next generation therapeutics. Also, many factors other than being non-self contribute to the immunogenicity of therapeutics (Yachnin et al., 2021), e.g. bacterially-derived non-immunoglobulin scaffolds such as affibodies have shown promising results for sustained therapy in clinical trials (Klint et al., 2023).

A major effort is under way to generate recombinant binders to the entire human proteome (Cao et al., 2022; Colwill et al., 2011; Dübel et al., 2010). The data here and elsewhere clearly illustrate how one binder is not enough and multiple binders to different regions of a target are valuable (Kast et al., 2021). Therefore, with an arsenal of tens of thousands of binders, methods such as SpyCombinator to screen the bispecific possibilities will accelerate the understanding and application of synergy for modulating cell signaling. Increasing numbers of functional proteins have been SpyTagged (Hentrich et al., 2021; Keeble and Howarth, 2019; Kellmann et al., 2023), allowing purification (Khairil Anuar et al., 2019; Vester et al., 2022), immobilization (Wang et al., 2020), multimerization (Brune and Howarth, 2018) and networking to other molecular functionalities (Keeble and Howarth, 2020). Beyond proteins, SpyTag/SpyCatcher has been functionalized with nucleic acids (Kröll et al., 2022), oligosaccharides (Li et al., 2022) or small molecules (Geissinger et al., 2020), which will allow modular assembly of bispecifics with more diverse activities. We anticipate applications of SpyCombinator beyond cell signaling, such as enhancing the recruitment of stem cells for tissue repair (Cousens et al., 2009) or optimizing enzyme networks for catalysis (Wei et al., 2020).

ACKNOWLEDGEMENTS

A.H.K. and M.H. were funded by the Biotechnology and Biological Sciences Research Council (BBSRC BB/S007369/1). C.L.D. was supported by the BBSRC Oxford Interdisciplinary Bioscience Doctoral Training Partnership (DTP) (grant number BB/T008784/1). We thank Dr. David Staunton from the University of Oxford Department of Biochemistry Biophysical Suite for help with biophysical analysis. We thank Dr. Anthony Tumber of University of Oxford Department of Chemistry for assistance with MS, supported by the BBSRC (BB/R000344/1).
For the purpose of Open Access, the author has applied a CC BY public copyright licence to any Author Accepted Manuscript (AAM) version arising from this submission.

AUTHOR CONTRIBUTIONS

C.L.D. performed all experiments. A.H.K. designed and purified initial constructs. C.L.D. and M.H. designed the project. C.L.D. and M.H. wrote the manuscript. All authors read and approved the manuscript.

DECLARATION OF INTERESTS

M.H. is an inventor on a patent on spontaneous amide bond formation (EP2534484) and a SpyBiotech co-founder and shareholder. M.H. and A.H.K. are inventors on a patent on SpyTag003/SpyCatcher003 (UK Intellectual Property Office 1706430.4). C.L.D., A.H.K. and M.H. are inventors on a patent application on the bispecific approach here (United Kingdom Patent Application No. 2313175.8).

Materials and Methods

Plasmids and Cloning

Constructs were cloned by PCR methods using Q5 High-Fidelity Polymerase (New England Biolabs) and fragments were assembled by Gibson assembly. All constructs were validated by Sanger Sequencing.

pET28a-SpyTag003-MBP (GenBank Accession no. MN433888, Addgene plasmid ID 133450), pET28-SpyTag003-mClover3 (Addgene plasmid ID 133453) (Keeble et al., 2019), pDEST14-SpyCatcher003 S49C (Addgene plasmid ID 133448) (Vester et al., 2022), pET28-MBP-super TEV protease (Addgene plasmid ID 171782) (Keeble et al., 2022), pET28a-SnoopTag-AffiHER2-SpyTag (N-terminal His_6–SnoopTag–anti-HER2 Affibody–SpyTag) (GenBank accession no. KU296975) (Addgene deposition in progress) (Brune et al., 2017), and pET28a-SnoopTag-SpyTag-$(AffiHER2)_3$ (GenBank accession no. KU296976) (Addgene deposition in progress) (Veggiani et al., 2016) have been described. pET28a-SUMO-SpyTag003 (N-terminal His_6 tag-SUMO protein-SpyTag003) was cloned previously by Irsyad Khairil Anuar (University of Oxford) (GenBank and Addgene deposition in progress). pDEST14-SpyCatcher003-TEVs-SpyTag003DA ('Masked SpyCatcher0003'; N-terminal His_6 tag-SpyCatcher003-TEV protease cleavage site-SpyTag003 D117A, GenBank and Addgene deposition in progress) was derived from pDEST14-SpyCatcher003 (GenBank Accession no. MN433887, Addgene plasmid ID 133447) by incorporating the TEV protease cleavage site (ENLYFQ/G) and SpyTag003 D117A (RGVPHIVMVAAYKRYK) (Keeble et al., 2019) by Gibson assembly. pDEST14-SpyCatcher003-$(GSG)_3$-SpyCatcher003-TEVs-SpyTag003DA (DoubleCatcher; N-terminal His_6 tag-TEV protease cleavage site-two SpyCatcher003 moieties connected by a $(GSG)_3$ spacer-TEV protease cleavage site-SpyTag003 DA, GenBank and Addgene deposition in progress) was synthesized as a gene fragment (Integrated DNA Technologies) and inserted into pDEST14. The Gly/Ser spacer in this construct was then replaced with an α-helical spacer (sequence PANLKALEAQKQKEQRQAAEELANAKKLKEQLEK) (Kuhlman et al., 1997), and this construct was termed DoubleCatcher H-Lock (GenBank and Addgene deposition in progress). Double-cysteine substitution variants of DoubleCatcher were derived from pDEST14-SpyCatcher003-$(GSG)_3$-SpyCatcher003-TEVs-SpyTag003DA by Gibson assembly: DoubleCatcher α-Lock (GenBank and Addgene deposition in progress), DoubleCatcher β-Lock (GenBank and Addgene deposition in progress), DoubleCatcher γ-Lock (GenBank and Addgene deposition in progress), DoubleCatcher δ-Lock (GenBank and Addgene deposition in progress), and DoubleCatcher ε-Lock (GenBank and Addgene deposition in progress). pET28a-MBP_X-MBP_X-SpyTag003 (His_6-MBP_X-SSSGGSGGGSG linker-MBP_X-SpyTag003; GenBank and Addgene deposition in progress), where MBP_X is a variant of MBP with stronger maltose binding (Veggiani et al., 2016), was cloned by Dr Henry Wood (University of Oxford). pcDNA3.1-Tras heavy chain-GSG-SpyTag003 ('Tras'), pcDNA3.1-Tras heavy chain-

589 SpyTag003 ('Tras NoLink') and pcDNA3.1-Tras light chain (GenBank and Addgene
590 deposition in progress) were cloned previously by Jamie Lam (University of Oxford) from
591 previous constructs in pOPIN, which have been described (Vester et al., 2022).
592 Sequences for the heavy and light chains of anti-HER2 Fabs were synthesized (Twist
593 Bioscience) and cloned into pcDNA3.1 plasmid: 39S (Oganesyan et al., 2018), MF3958
594 (Geuijen et al., 2018), H2-18 (Hu et al., 2015), HFS2 (Salimi et al., 2018) and Pert (Gennaro
595 et al., 2014). Each Fab heavy chain had the final assembly: N-terminal signal peptide-Heavy
596 variable domain-Human IgG1 C_H1 domain-EPKSC IgG1 upper hinge region residues-
597 SpyTag003-His_6 tag, with the exception of HSF2 whose C_H1 domain was of mouse origin, and
598 Pert for which the hinge region was omitted (GenBank and Addgene deposition in progress).
599 Each Fab light chain had the final assembly: N-terminal signal peptide-Light variable domain-
600 Human kappa light chain, with the exception of HSF2 whose kappa light chain was of mouse
601 origin. pET28a-nanoHER2-SpyTag003 (GenBank and Addgene deposition in progress), based
602 on the 11A4 nanobody against HER2 (Verheije et al., 2013), was cloned with a C-terminal His_6
603 tag.
604
605 **Bacterial Protein Expression**
606 pDEST14 constructs were transformed into chemically competent *E. coli* C41 (DE3), a gift
607 from Anthony Watts (University of Oxford), except for the pDEST14-SpyCatcher003-
608 SpyCatcher003-TEV site-SpyTag003DA disulfide-containing variants, which were
609 transformed into chemically competent *E. coli* T7SHuffle (NEB). pET28a and pETDuet
610 constructs were transformed into chemically competent *E. coli* BL21 (DE3) (Agilent
611 Technologies), with the exception of pET28a-SnoopTag-AffiHER2-SpyTag, which was
612 transformed into chemically competent *E. coli* T7 Express (NEB). Colonies were picked into
613 10 mL LB containing either 100 µg/mL ampicillin (pDEST14/pETDuet) or 25-50 µg/mL
614 kanamycin (pET28a), and grown at 37 °C at 200 rpm for 4-16 h. Starter cultures were diluted
615 100-fold into either 1 L LB supplemented with appropriate antibiotic and 0.8% (w/v) glucose,
616 1 L LB supplemented with antibiotic alone (T7 Express only), or 2 × TY supplemented with
617 antibiotic and 0.5% (v/v) glycerol (T7SHuffle only), and grown at 37 °C with shaking at 200
618 rpm. At OD_{600} 0.5-0.6, expression was induced with 0.42 mM isopropyl β-D-1-
619 thiogalactopyranoside (IPTG; Fluorochem). pDEST14-transformed cultures were then
620 incubated for 4 h at 30 °C and 200 rpm, while all other cultures were incubated for 16 h at 18
621 °C and 200 rpm post-induction. Cells were harvested by centrifugation at 4,000 *g* for 15 min
622 at 4 °C and pellets were stored at -80 °C until purification.
623
624 **Mammalian Protein Expression**
625 Anti-HER2 Fabs were expressed in Expi293F cells (Thermo Fisher), which were maintained
626 in Expi293 Expression Medium (Thermo Fisher) supplemented with 50 U/mL penicillin and
627 50 µg/mL streptomycin and grown in a humidified Multitron Cell incubator (Infors HT) at 37
628 °C with 8% (v/v) CO_2 and shaking at either 125 rpm (125 mL flasks; Corning) or 240 rpm (50
629 mL mini bioreactor tubes; Corning). After ≥ 3 passages, cells were diluted to 3×10^6 cells/mL
630 in antibiotic-free Expi293 Expression Medium and transfected using an ExpiFectamine 293
631 Transfection Kit (Thermo Scientific). ExpiFectamine 293 Transfection Enhancers 1 and 2 were
632 added 20 h post transfection and cultures were incubated for 5 days post-transfection, when
633 cell viability fell below 50%. Cell supernatants were supplemented with cOmplete, Mini,
634 EDTA-free Protease Inhibitor Cocktail (Roche) and clarified by centrifugation at 4,000 *g* at 4
635 °C, followed by filtration through a 0.22 µm syringe filter (Thermo Fisher). One tenth
636 supernatant volume of Ni-NTA wash buffer (50 mM Tris-HCl pH 7.8, 300 mM NaCl, 10 mM
637 imidazole) was added to filtered supernatant, which was then pH-adjusted to pH 7.6 using 1 M

638 Tris-HCl pH 8.0. Supernatants were stored at -80 °C until purification. The typical yield for
639 SpyTag003-fused Fabs ranged from 6 to 156 mg per L of culture.
640
641 **Ni-NTA purification of His$_6$-tagged proteins**
642 After thawing, bacterial cell pellets were resuspended in 1× Ni-NTA buffer (50 mM Tris-HCl
643 pH 7.8, 300 mM NaCl) supplemented with cOmplete, Mini, EDTA-free Protease Inhibitor
644 Cocktail (Roche) and 1 mM phenylmethylsulfonyl fluoride (PMSF), and lysed by sonication
645 on ice. SpyCatcher003 S49C variants and DoubleCatcher double-cysteine variants were further
646 supplemented with 10 mM 2-mercaptoethanol to break disulfide bonds to other proteins.
647 Clarified cell lysates were centrifuged at 30,000 *g* for 30 min at 4 °C and adjusted to pH 7.6
648 using 1 M Tris-HCl pH 8.0, before purification by Ni-NTA affinity chromatography (Qiagen)
649 as previously described (Fierer et al., 2014). Elution of all proteins was performed in the
650 absence of 2-mercaptoethanol. For anti-HER2 binding proteins to be heterodimerized by
651 DoubleCatcher for treatment of cells, the following washes were performed directly prior to
652 elution: 50 column volumes (CV) wash buffer containing 0.1% (v/v) Triton X-114 (50 mM
653 Tris-HCl pH 7.8, 300 mM, 10 mM imidazole), followed by 10 CV wash buffer (50 mM Tris-
654 HCl pH 7.8, 300 mM). Clarified mammalian supernatants were purified identically. Eluted
655 proteins were dialyzed three times against PBS pH 7.4 (137 mM NaCl, 2.7 mM KCl, 10 mM
656 Na_2HPO_4, 1.8 mM KH_2PO_4) in 3.5 kDa molecular weight cut-off Spectra/Por tubing (Spectrum
657 Labs) at 4 °C. SpyCatcher003 S49C variants to be coupled to resin were instead dialyzed into
658 coupling buffer (50 mM Tris-HCl pH 8.5, 5 mM EDTA). Protein concentrations were
659 determined from A_{280} using their predicted extinction coefficient from ExPASy ProtParam.
660 Typical yield for SpyCatcher003-containing variants was 10-20 mg per L of culture. A typical
661 yield for affibody expression was ~3 mg per L of culture, and 30 mg per L for nanobody
662 expressions. Expression of SpyTag003-fused, non-antigen binding proteins yielded 5-15 mg
663 protein per L of culture.
664 Prior to assembly of bispecific molecules with DoubleCatcher for mammalian cell
665 treatment, endotoxin was removed from DoubleCatcher scaffolds by phase separation with
666 Triton X-114 (Aida and Pabst, 1990). Purified protein samples were transferred to 1.5 mL
667 endotoxin-free microcentrifuge tubes (StarLab, cat. E1415−1510), to which 1% (v/v) Triton
668 X-114 was added. Samples were incubated on ice for 5 min, until all Triton X-114 was
669 dissolved. Samples were then incubated at 37 °C for 5 min and centrifuged for 1 min at 16,000
670 *g* at 37 °C. The supernatant was pipetted off, and the entire procedure was repeated twice.
671 Endotoxin concentration of any bispecific constituent to be added to cells was determined using
672 the Limulus amebocyte lysate (LAL) Chromogenic Endotoxin Quantitation Kit (Thermo
673 Fisher) according to the manufacturer's instructions, which confirmed the endotoxin level to
674 be below 1 endotoxin unit/mL.
675
676 **SpySwitch purification of SpyTag003-tagged proteins**
677 MBP$_X$-MBP$_X$-SpyTag003 cell pellets were lysed and clarified as outlined above, except
678 thawed pellets were resuspended in 1 × SpySwitch buffer (50 mM Tris-HCl pH 7.5, 300 mM
679 NaCl). SpySwitch purification was performed at 4 °C, as described previously (Vester et al.,
680 2022). Briefly, SpySwitch resin (0.75 mL per 1 L bacterial culture) was equilibrated with 2×10
681 CV SpySwitch buffer, prior to incubation with clarified cell lysate on an end-over-end rotator
682 for 1 h at 4 °C, after which resin was washed with 4 × 10 CV SpySwitch buffer. pH-dependent
683 elution was performed by incubating the resin with 6 × 1.5 CV SpySwitch elution buffer (50
684 mM acetic acid, 150 mM NaCl, pH 5.0) for 5 min each, which was immediately neutralized by
685 mixing the flow-through with 6 × 0.3 CV of 1 M Tris-HCl pH 8.0. Proteins were subsequently
686 dialyzed into PBS pH 7.4.
687

688 **Polyacrylamide gel electrophoresis**
689 SDS-PAGE was performed using 8-16% polyacrylamide gels in an XCell SureLock system
690 (Thermo Scientific). SDS-PAGE was run at 200 V in 25 mM Tris-HCl pH 8.5, 192 mM
691 glycine, 0.1% (w/v) SDS. Gels were stained with Brilliant Blue G-250 and destained with
692 Milli-Q H_2O prior to imaging on a ChemiDoc XRS+ imager. ImageLab 6.1.0 software (Bio-
693 Rad) was used for densitometric quantification of bands. For imaging on an iBright FL1500
694 imaging system (Thermo Fisher), analysis was performed using iBright Analysis Software
695 Versions 5.0.1 and 5.2.0 (Thermo Fisher).
696
697 **Size-Exclusion Chromatography**
698 Ni-NTA- or SpySwitch-purified protein samples (SpyCatcher003-containing variants,
699 SpyTag003-linked non-antigen binding proteins) were injected onto a pre-equilibrated HiLoad
700 16/600 Superdex 200 pg column (GE Healthcare), or a HiLoad 16/600 Superdex 75 pg column
701 (SUMO-SpyTag003 and affibodies; GE Healthcare). Samples were run on an ÄKTA Pure 25
702 (GE Healthcare) fast protein liquid chromatography machine at 1 mL/min in PBS pH 7.4 at 4
703 °C. The absorbance profile of column elutions was recorded at 230 nm, 260 nm, and 280 nm.
704 Each column was calibrated using 660 kDa to 1.35 kDa molecular weight protein standards
705 (thyroglobulin, IgG, ovalbumin, myoglobin, and vitamin B12) (Bio-Rad). Following peak
706 analysis by SDS-PAGE, fractions containing purified protein at the expected molecular weight
707 were concentrated using Vivaspin 20 centrifugal filters (Cytiva) at 4 °C and then stored at -80
708 °C.
709
710 **Resin coupling**
711 SpyCatcher003 S49C was attached to SulfoLink Coupling Resin (Thermo Fisher) according to
712 the manufacturer's instructions, with the following changes: SpyCatcher003 S49C in coupling
713 buffer was concentrated to 20 mg/mL using a Vivaspin 20 5 kDa molecular weight cut-off
714 centrifugal filter at 4 °C, reduced with 1 mM tris(2-carboxyethyl)phosphine (TCEP) for 30 min
715 at 25 °C, and coupled to SulfoLink Coupling Resin at 20 mg reduced protein per mL of packed
716 resin. Following washes with 1 M NaCl, the coupled resin was washed with TP buffer (25 mM
717 orthophosphoric acid adjusted to pH 7.0 with Tris base) to remove SpyCatcher003 S49C that
718 had bound non-covalently to the resin. The coupled resin was stored in 20% (v/v) ethanol in
719 PBS pH 7.4 at 4 °C for ≤ 3 months.
720
721 **Isopeptide bond reconstitution reactions**
722 All reactions were carried out in triplicate in PBS pH 7.4. 2.5 µM SpyCatcher003 (at 25 °C),
723 Masked SpyCatcher003, or DoubleCatcher variants (each at 37 °C) was reacted with 5 µM
724 SpyTag003-linked protein. At each time-point or end-point indicated, reactions were quenched
725 by adding 6 × SDS loading buffer [0.23 M Tris-HCl pH 6.8, 24% (v/v) glycerol, 120 µM
726 bromophenol blue, 0.23 M SDS], with subsequent heating at 95 °C for 5 min in a Bio-Rad
727 C1000 thermal cycler. Reactions were analyzed by SDS-PAGE and the depletion of
728 SpyCatcher003-derived reactant over time was quantified by densitometry. The extent of
729 reaction between binding partners at each time point is defined as 100 × [1 - (SpyCatcher003-
730 derived reactant)/(average density of SpyCatcher003-derived reactant in control lanes)].
731
732 **Assembly of dimeric molecules using DoubleCatcher**
733 With the exception of reconstitution assays, the assembly of bispecific molecules from two
734 SpyTag(003)-linked proteins of interest, 'Protein A' and 'Protein B', was performed in 100 µL
735 total volume per well in 96-well cell culture plates (Thermo Scientific, cat. 167008): 1)
736 DoubleCatcher variant with concentration N (here, N = 1–75 µM) was first mixed with 1.25 ×
737 N Protein A-SpyTag003 for 2 h at 25 °C with shaking at 550 rpm; 2) 5 × N Protein B-

SpyTag003 and 1/12 × *N* MBP-superTEV was added directly to the reaction mixture and incubated for 4 h at 34 °C with shaking at 550 rpm; 3) reaction mixture was incubated with SulfoLink resin-immobilized SpyCatcher003 S49C for 16 h at 4 °C with shaking at 550 rpm, to remove excess unreacted SpyTag003-linked binders from solution. All coupling reactions were carried out in PBS pH 7.4.

Dynamic Light Scattering

Size-exclusion chromatography-purified protein samples were centrifuged for 30 min at 16,900 *g* at 4 °C to remove any aggregates. Samples were filtered through 0.33 mm diameter sterile syringe filters with a 0.22 µm hydrophilic polyvinylidene difluoride (PVDF) membrane (Sigma-Aldrich) and diluted to a final concentration of 25 µM for protein samples > 35 kDa, or 75 µM for samples < 35 kDa into sterile filtered PBS pH 7.4. 20 µL diluted sample was loaded into a reusable quartz cuvette and measurements (10 scans of 10 s each) were recorded at 20 °C using an Omnisizer (Viscotek). Data were analyzed in duplicate using OmniSIZE 3.0. For each sample, the radius of hydration (R_h) was plotted with error bars ± 1 s.d.

Cell Culture

SKBR3 cells were from ATCC. BT474 cells were from Cancer Research UK, Lincoln's Inn Fields. SKBR3 cells were grown in complete DMEM: Dulbecco's Modified Eagle Medium–high glucose (DMEM) supplemented with 10% (v/v) fetal bovine serum (FBS), 100 U/mL penicillin and 100 µg/mL streptomycin (1 × pen/strep; Sigma-Aldrich), 1% (v/v) GlutaMAX (Thermo Fisher Scientific) at 37 °C and 5% (v/v) CO_2. BT474 cells were grown in complete RPMI: RPMI-1640 supplemented with 10% fetal bovine serum (FBS), 100 U/mL penicillin and 100 µg/mL streptomycin (1 × pen/strep; Sigma-Aldrich), and insulin (5 µg/mL; Sigma) at 37 °C and 5% (v/v) CO_2. Cells were passaged at 70-80% confluency and were sub-cultured for fewer than 3 months. Cell-lines were validated as mycoplasma-negative by PCR.

Metabolic Activity Assay

BT474 or SKBR3 cells were seeded into 96-well plates at 1.25×10^4 cells per well and grown in DMEM supplemented with 0.5% (v/v) FBS, 1% (v/v) GlutaMAX and 50 U/mL penicillin and 50 µg/mL streptomycin (0.5 × pen/strep) at 37 °C for 24 h. 100 nM and subsequent serial dilutions of anti-HER2 binders coupled to DoubleCatcher were prepared in 125 µL DMEM with 0.1% (v/v) FBS, 1% (v/v) GlutaMAX and 0.5 × pen/strep. Spent media was removed and protein solutions were added to cells. DoubleCatcher or MBP-superTEV alone were applied to cells at the same concentrations as the anti-HER2 binders as a negative control for cell killing. Cells were treated for 96 h at 37 °C with 5% (v/v) CO_2, after which 40 µL 0.15 mg/mL Resazurin (Alamar Blue; Sigma-Aldrich) prepared in PBS pH 7.4 and dissolved in PBS and sterile-filtered through a 0.22 µm pore-sized membrane filter was added directly to each well, and plates were incubated for 4 h at 37 °C with 5% (v/v) CO_2. Fluorescence (λ_{ex} 544 nm, λ_{em} 590 nm) was measured using a FLUOstar Omega plate reader (BMG Labtech). The fluorescence intensity of media, without cells, containing Resazurin ('background') was subtracted from each measurement. The percent metabolic activity relative to untreated cells was then defined as 100 × (background-subtracted fluorescence of cells)/(background-subtracted fluorescence of untreated cells). Untreated cells are defined as cells grown in DMEM + 1% (v/v) FBS, 0.5 × pen/strep alone.

Mass Spectrometry

Intact protein mass spectrometry in positive ion mode was performed using a RapidFire 365 jet-stream electrospray ion source (Agilent) coupled to a 6550 Accurate-Mass Quadrupole Time-of-Flight (Q-TOF) (Agilent) mass spectrometer. 50 µL protein samples at 10 µM in PBS

788 pH 7.4 were prepared on a 384-well polypropylene plate (Greiner). Samples were acidified to
789 1% (v/v) formic acid, before aspiration under vacuum for 0.4 s and loading onto a C4 solid-
790 phase extraction cartridge. Following washes with 0.1% (v/v) formic acid in water (1.5 mL/min
791 flow rate for 5.5 s), samples were eluted to the Q-TOF detector with deionized water containing
792 85% (v/v) acetonitrile and 0.1% (v/v) formic acid (1.25 mL/min flow rate for 5.5 s). Data were
793 analyzed using Mass Hunter Qualitative Analysis software B.07.00 (Agilent). Expected
794 molecular weights for full-length proteins were calculated using the ExPASy ProtParam tool,
795 with the N-terminal fMet (bacterial expression) or signal peptide sequence (mammalian
796 expression) removed. Signal peptide cleavage was predicted by SignalP 6.0 (Nielsen et al.,
797 2019). -2 Da was calculated for each predicted disulfide bond. The small amount of +178 Da
798 peak relates to gluconoylation, a common spontaneous post-translational modification for
799 proteins overexpressed in *E. coli* BL21 (Geoghegan et al., 1999).
800
801 **Mass Photometry**
802 Microscope coverslips (24 × 50 mm, Menzel Gläser) were cleaned by sequential sonication in
803 50% (v/v) isopropanol and Milli-Q H_2O (5 min each), dried under a clean nitrogen stream, and
804 assembled into flow chambers with isopropanol/Milli-Q H_2O-rinsed and nitrogen-dried
805 silicone gaskets (6 mm × 1 mm, GBL103280, Grace Bio-Labs) as outlined (Young et al., 2018).
806 Data were acquired on a Refeyn TwoMP mass photometer. Immediately prior to mass
807 photometry, protein samples were diluted into freshly prepared and degassed MP sample buffer
808 [PBS pH 7.4, 300 mM NaCl, 0.5% (v/v) glycerol, 1 mM NaN_3, sterile-filtered through a 0.22
809 µm pore-size syringe filter (Thermo Fisher)]. A dynamin protein mass standard (MS1000 20-
810 40×), diluted into MP sample buffer, was used to calibrate the mass photometer each time a
811 new cover slip was used (Foley et al., 2021). The focal position of the microscope was found
812 in flow chambers containing 20 µL sample, after which 0.5-10 µL of MP sample buffer was
813 replaced with an equivalent volume protein sample, to a final working concentration of 2-50
814 nM, to account for differences in the dissociation characteristics of different proteins. After ≤
815 10 s, images were acquired for 60 s at 331 Hz. Each sample was measured at least twice
816 independently. All data were processed using DiscoverMP v1.2.3 software (Refeyn Ltd) (Foley
817 et al., 2021). Masses were plotted as mass histogram (bin width = 2.5 kDa) and fitted to
818 Gaussian non-linear regression curves to identify the mean masses of each protein
819 subpopulation within the heterogeneous sample in GraphPad Prism 9 (GraphPad Software).
820 Expected molecular weights for protein constituents were calculated using the ExPASy
821 ProtParam tool, with the N-terminal fMet (bacterial expression) or signal peptide sequence
822 (mammalian expression) removed.
823
824 **Data Analysis and Graphics Visualization**
825 Data visualization and statistical tests were performed using GraphPad Prism 9 (GraphPad
826 Software) and MATLAB R2023a (Mathworks). Protein structures were visualized using
827 PyMOL 2.5.4 (Schrödinger). The structure of HER2 was assembled in PyMOL from PDB IDs
828 1N8Z (Extracellular Domain) (Cho et al., 2003), 2KS1 (transmembrane domain) (Mineev et
829 al., 2010), and 3PP0 (kinase domain) (Aertgeerts et al., 2011) as previously (Goodsell, 2022).
830 Binder structures are based on the following: Tras by PDB ID 1N8Z (Cho et al., 2003); Pert
831 by PDB ID 1S78 (Franklin et al., 2004); 39S by PDB ID 6ATT (Oganesyan et al., 2018);
832 MF3958 by PDB ID 5O4G (Geuijen et al., 2018); H2-18 by PDB ID 3WLW (Hu et al., 2015);
833 and AffiHER2 by PDB ID 3MZW (Eigenbrot et al., 2010). Protein structures for
834 DoubleCatcher variants were predicted using ColabFold versions 1.3 and 1.5.2 (Mirdita et al.,
835 2022), and structures for HER2 extracellular domain in complex with HFS2 or nanoHER2
836 were predicted using ColabFold version 1.4 (Mirdita et al., 2022). Structural predictions were
837 performed using the full-length protein sequence, except for HFS2 where the signal peptide

was removed. For all ColabFold-simulated structures, the structure predicted with the highest confidence is presented.

To simulate vectors that reflect the directionality of SpyTag003, the PyMOL modevectors tool was used to connect Ser57 to His53 and Ser179 to His175 by their carbonyl main-chain oxygens (Law, 2020) (DoubleCatcher numbering, according to sequence listed in Supplementary Fig. 1). The arrowhead represents the N-terminus of the SpyTag003 peptide, such that a binder with a C-terminal SpyTag003 would project from the arrowhead of the vector when it is coupled to DoubleCatcher.

Statistics and reproducibility

Statistical significance for metabolic activity assays were calculated by two-way analysis of variance (ANOVA) with Dunnett's correction for multiple comparison. For representative SDS-PAGE (Fig. 1C, E; Fig. 2B, E; Supplementary Fig. 4A, B), observations were confirmed at least once with similar or identical conditions. For Fig. 3 D, E, heterodimer assembly and subsequent analyses by mass photometry and SDS-PAGE were repeated at least twice with similar results. For Fig. 4C, D and Fig. 6D, the bispecific assemblies and subsequent metabolic activity assays were repeated at least twice independently with similar results. No statistical method was used to predetermine sample size. No data were excluded from the analyses. The experiments were not randomized. The Investigators were not blinded to allocation during experiments and outcome assessment.

Data availability

Amino acid sequences of Masked SpyCatcher003-containing variants are available in Supplementary Fig. 1. Sequences of other constructs are available in GenBank as described in the section Plasmids and cloning. Plasmids encoding DoubleCatchers and related binders will be deposited in the Addgene repository (https://www.addgene.org/Mark_Howarth/). Further information and request for resources and reagents should be directed to and will be fulfilled by the lead contact, M.H..

References

Aertgeerts, K., Skene, R., Yano, J., Sang, B.-C., Zou, H., Snell, G., Jennings, A., Iwamoto, K., Habuka, N., Hirokawa, A., et al. (2011). Structural Analysis of the Mechanism of Inhibition and Allosteric Activation of the Kinase Domain of HER2 Protein. J. Biol. Chem. *286*, 18756–18765.

Aida, Y., and Pabst, M.J. (1990). Removal of endotoxin from protein solutions by phase separation using triton X-114. J. Immunol. Methods *132*, 191–195.

Andres, F., Schwill, M., Boersma, Y.L., and Plückthun, A. (2020). High-throughput generation of bispecific binding proteins by sortase a-mediated coupling for direct functional screening in cell culture. Mol. Cancer Ther. *19*, 1080–1088.

Arkhipov, A., Shan, Y., Kim, E.T., Dror, R.O., and Shaw, D.E. (2013). Her2 activation mechanism reflects evolutionary preservation of asymmetric ectodomain dimers in the human EGFR family. Elife *2013*, 1–14.

Asor, R., and Kukura, P. (2022). Characterising biomolecular interactions and dynamics with mass photometry. Curr. Opin. Chem. Biol. *68*, 102132.

Baker, D. (2019). What has de novo protein design taught us about protein folding and biophysics? Protein Sci. *28*, 678–683.

885 Batada, N.N., Shepp, L.A., Siegmund, D.O., and Levitt, M. (2006). Spatial Regulation and
886 the Rate of Signal Transduction Activation. PLoS Comput. Biol. *2*, e44.

887 Brack, S., Attinger-Toller, I., Schade, B., Mourlane, F., Klupsch, K., Woods, R., Hachemi,
888 H., Von Der Bey, U., Koenig-Friedrich, S., Bertschinger, J., et al. (2014). A bispecific HER2-
889 targeting fynomAb with superior antitumor activity and novel mode of action. Mol. Cancer
890 Ther. *13*, 2030–2039.

891 Brockhoff, G., Schlegel, J., Heiß, P., Hofstaedter, F., and Knuechel, R. (2001). Epidermal
892 growth factor receptor, c-erbB2 and c-erbB3 receptor interaction, and related cell cycle
893 kinetics of SK-BR-3 and BT474 breast carcinoma cells. Cytometry *44*, 338–348.

894 Brune, K.D., and Howarth, M. (2018). New Routes and Opportunities for Modular
895 Construction of Particulate Vaccines: Stick, Click, and Glue. Front. Immunol. *9*, 1432.

896 Brune, K.D., Buldun, C.M., Li, Y., Taylor, I.J., Brod, F., Biswas, S., and Howarth, M.
897 (2017). Dual Plug-and-Display Synthetic Assembly Using Orthogonal Reactive Proteins for
898 Twin Antigen Immunization. Bioconjug. Chem. *28*, 1544–1551.

899 Cabrita, L.D., Gilis, D., Robertson, A.L., Dehouck, Y., Rooman, M., and Bottomley, S.P.
900 (2007). Enhancing the stability and solubility of TEV protease using in silico design. Protein
901 Sci. *16*, 2360–2367.

902 Cao, L., Coventry, B., Goreshnik, I., Huang, B., Sheffler, W., Park, J.S., Jude, K.M.,
903 Marković, I., Kadam, R.U., Verschueren, K.H.G., et al. (2022). Design of protein-binding
904 proteins from the target structure alone. Nature *605*, 551–560.

905 Cao, Y., Liu, D., and Zhang, W. Bin (2017). Supercharging SpyCatcher toward an
906 intrinsically disordered protein with stimuli-responsive chemical reactivity. Chem. Commun.
907 *53*, 8830–8833.

908 Chen, J., Huang, C., Zhao, W., Ren, J., Ji, F., and Jia, L. (2022). SnoopLigase Enables Highly
909 Efficient Generation of C–C-Linked Bispecific Nanobodies Targeting TNF-α and IL-17A.
910 Bioconjug. Chem. *33*, 1446–1455.

911 Cho, H.-S.S., Mason, K., Ramyar, K.X., Stanley, A.M., Gabelli, S.B., Denney, D.W., and
912 Leahy, D.J. (2003). Structure of the extracellular region of HER2 alone and in complex with
913 the Herceptin Fab. Nature *421*, 756–760.

914 Colwill, K., Gräslund, S., Persson, H., Jarvik, N.E., Wyrzucki, A., Wojcik, J., Koide, A.,
915 Kossiakoff, A.A., Koide, S., Sidhu, S., et al. (2011). A roadmap to generate renewable
916 protein binders to the human proteome. Nat. Methods *8*, 551–561.

917 Cousens, L.P., Terry, F.E., and Falanga, V. (2009). New Applications for Bispecific
918 Antibodies in Wound Healing (94.16). J. Immunol. *182*, 94.16-94.16.

919 Dengl, S., Mayer, K., Bormann, F., Duerr, H., Hoffmann, E., Nussbaum, B., Tischler, M.,
920 Wagner, M., Kuglstatter, A., Leibrock, L., et al. (2020). Format chain exchange (FORCE) for
921 high-throughput generation of bispecific antibodies in combinatorial binder-format matrices.
922 Nat. Commun. *11*, 4974.

923 Dübel, S., Stoevesandt, O., Taussig, M.J., and Hust, M. (2010). Generating recombinant
924 antibodies to the complete human proteome. Trends Biotechnol. *28*, 333–339.

925 Eigenbrot, C., Ultsch, M., Dubnovitsky, A., Abrahmsén, L., and Härd, T. (2010). Structural
926 basis for high-affinity HER2 receptor binding by an engineered protein. Proc. Natl. Acad.
927 Sci. U. S. A. *107*, 15039–15044.

928 Feldwisch, J., Tolmachev, V., Lendel, C., Herne, N., Sjöberg, A., Larsson, B., Rosik, D.,

929 Lindqvist, E., Fant, G., Höidén-Guthenberg, I., et al. (2010). Design of an Optimized
930 Scaffold for Affibody Molecules. J. Mol. Biol. *398*, 232–247.

931 Foley, E.D.B., Kushwah, M.S., Young, G., and Kukura, P. (2021). Mass photometry enables
932 label-free tracking and mass measurement of single proteins on lipid bilayers. Nat. Methods
933 *18*, 1247–1252.

934 Franklin, M.C., Carey, K.D., Vajdos, F.F., Leahy, D.J., de Vos, A.M., and Sliwkowski, M.X.
935 (2004). Insights into ErbB signaling from the structure of the ErbB2-pertuzumab complex.
936 Cancer Cell *5*, 317–328.

937 Freed, D.M., Bessman, N.J., Kiyatkin, A., Salazar-Cavazos, E., Byrne, P.O., Moore, J.O.,
938 Valley, C.C., Ferguson, K.M., Leahy, D.J., Lidke, D.S., et al. (2017). EGFR Ligands
939 Differentially Stabilize Receptor Dimers to Specify Signaling Kinetics. Cell *171*, 683-
940 695.e18.

941 Geissinger, S.E., Schreiber, A., Huber, M.C., Stühn, L.G., and Schiller, S.M. (2020).
942 Adjustable Bioorthogonal Conjugation Platform for Protein Studies in Live Cells Based on
943 Artificial Compartments. ACS Synth. Biol. *9*, 827–842.

944 Gennaro, L.A., Kao, Y.-H., and Zhang, Y. (2014). PERTUZUMAB VARIANTS AND
945 EVALUATION THEREOF. US patent application US 20140308277A1.

946 Geuijen, C.A.W., De Nardis, C., Maussang, D., Rovers, E., Gallenne, T., Hendriks, L.J.A.,
947 Visser, T., Nijhuis, R., Logtenberg, T., de Kruif, J., et al. (2018). Unbiased Combinatorial
948 Screening Identifies a Bispecific IgG1 that Potently Inhibits HER3 Signaling via HER2-
949 Guided Ligand Blockade. Cancer Cell *33*, 922-936.e10.

950 Goodsell, D.S. (2022). HER2/neu and Trastuzumab. https://pdb101.rcsb.org/motm/268.
951 (Accessed 11 January 2023).

952 Gray, D.C., Mahrus, S., and Wells, J.A. (2010). Activation of specific apoptotic caspases
953 with an engineered small-molecule-activated protease. Cell *142*, 637–646.

954 Gu, J., Yang, J., Chang, Q., Lu, X., Wang, J., Chen, M., Ghayur, T., and Gu, J. (2014).
955 Identification of Anti-ErbB2 Dual Variable Domain Immunoglobulin (DVD-Ig^{TM}) Proteins
956 with Unique Activities. PLoS One *9*, e97292.

957 Han, L., Chen, J., DIng, K., Zong, H., Xie, Y., Jiang, H., Zhang, B., Lu, H., Yin, W., Gilly, J.,
958 et al. (2017). Efficient generation of bispecific IgG antibodies by split intein mediated protein
959 trans-splicing system. Sci. Rep. *7*, 1–11.

960 Hartzell, E.J., Terr, J., and Chen, W. (2021). Engineering a Blue Light Inducible SpyTag
961 System (BLISS). J. Am. Chem. Soc. *143*, 8572–8577.

962 Hendriks, B.S., Klinz, S.G., Reynolds, J.G., Espelin, C.W., Gaddy, D.F., and Wickham, T.J.
963 (2013). Impact of tumor HER2/ERBB2 expression level on HER2-targeted liposomal
964 doxorubicin-mediated drug delivery: Multiple low-affinity interactions lead to a threshold
965 effect. Mol. Cancer Ther. *12*, 1816–1828.

966 Hentrich, C., Kellmann, S.-J., Putyrski, M., Cavada, M., Hanuschka, H., Knappik, A., and
967 Ylera, F. (2021). Periplasmic expression of SpyTagged antibody fragments enables rapid
968 modular antibody assembly. Cell Chem. Biol. *28*, 813-824.e6.

969 Hofmann, T., Krah, S., Sellmann, C., Zielonka, S., and Doerner, A. (2020). Greatest hits—
970 innovative technologies for high throughput identification of bispecific antibodies. Int. J.
971 Mol. Sci. *21*, 1–17.

972 Hu, S., Sun, Y., Meng, Y., Wang, X., Yang, W., Fu, W., Guo, H., Qian, W., Hou, S., Li, B.,

et al. (2015). Molecular architecture of the ErbB2 extracellular domain homodimer. Oncotarget *6*, 1695–1706.

Jain, J., Veggiani, G., and Howarth, M. (2013). Cholesterol loading and ultrastable protein interactions determine the level of tumor marker required for optimal isolation of cancer cells. Cancer Res. *73*, 2310–2321.

Junttila, T.T., Akita, R.W., Parsons, K., Fields, C., Lewis Phillips, G.D., Friedman, L.S., Sampath, D., and Sliwkowski, M.X. (2009). Ligand-Independent HER2/HER3/PI3K Complex Is Disrupted by Trastuzumab and Is Effectively Inhibited by the PI3K Inhibitor GDC-0941. Cancer Cell *15*, 429–440.

Kamashev, D., Shaban, N., Suntsova, M., Raevskiy, M., Efimov, V., Moisseev, A., Sorokin, M., and Buzdin, A. (2022). Human Blood Serum Inhibits Ductal Carcinoma Cells BT474 Growth and Modulates Effect of HER2 Inhibition. Biomedicines *10*, 1914.

Kast, F., Schwill, M., Stüber, J.C., Pfundstein, S., Nagy-Davidescu, G., Rodríguez, J.M.M., Seehusen, F., Richter, C.P., Honegger, A., Hartmann, K.P., et al. (2021). Engineering an anti-HER2 biparatopic antibody with a multimodal mechanism of action. Nat. Commun. *12*, 3790.

Keeble, A.H., and Howarth, M. (2019). Insider information on successful covalent protein coupling with help from SpyBank. In Methods in Enzymology, (Elsevier Inc.), pp. 443–461.

Keeble, A.H., and Howarth, M. (2020). Power to the protein: Enhancing and combining activities using the Spy toolbox. Chem. Sci. *11*, 7281–7291.

Keeble, A.H., Turkki, P., Stokes, S., Anuar, I.N.A.K., Rahikainen, R., Hytönen, V.P., and Howarth, M. (2019). Approaching infinite affinity through engineering of peptide-protein interaction. Proc. Natl. Acad. Sci. U. S. A. *116*, 26523–26533.

Keeble, A.H., Yadav, V.K., Ferla, M.P., Bauer, C.C., Chuntharpursat-Bon, E., Huang, J., Bon, R.S., and Howarth, M. (2022). DogCatcher allows loop-friendly protein-protein ligation. Cell Chem. Biol. *29*, 339-350.e10.

Kellmann, S.-J., Hentrich, C., Putyrski, M., Hanuschka, H., Cavada, M., Knappik, A., and Ylera, F. (2023). SpyDisplay: A versatile phage display selection system using SpyTag/SpyCatcher technology. MAbs *15*, 2003–2005.

Khairil Anuar, I.N.A., Banerjee, A., Keeble, A.H., Carella, A., Nikov, G.I., and Howarth, M. (2019). Spy&Go purification of SpyTag-proteins using pseudo-SpyCatcher to access an oligomerization toolbox. Nat. Commun. *10*, 1734.

Ki, H., Jo, J., Kim, Y., Kim, T.W., Kim, C., Kim, Y., Kim, C.W., Muniyappan, S., Lee, S.J., Kim, Y., et al. (2021). Uncovering the Conformational Distribution of a Small Protein with Nanoparticle-Aided Cryo-Electron Microscopy Sampling. J. Phys. Chem. Lett. *12*, 6565–6573.

Kirouac, D.C., Du, J., Lahdenranta, J., Onsum, M.D., Nielsen, U.B., Schoeberl, B., and McDonagh, C.F. (2016). HER2+ Cancer Cell Dependence on PI3K vs. MAPK Signaling Axes Is Determined by Expression of EGFR, ERBB3 and CDKN1B. PLOS Comput. Biol. *12*, e1004827.

Klint, S., Feldwisch, J., Gudmundsdotter, L., Dillner Bergstedt, K., Gunneriusson, E., Höidén Guthenberg, I., Wennborg, A., Nyborg, A.C., Kamboj, A.P., Peloso, P.M., et al. (2023). Izokibep: Preclinical development and first-in-human study of a novel IL-17A neutralizing Affibody molecule in patients with plaque psoriasis. MAbs *15*, 2209920.

Kröll, S., Schneider, L., Wadhwani, P., Rabe, K.S., and Niemeyer, C.M. (2022). Orthogonal

1017 protein decoration of DNA nanostructures based on SpyCatcher-SpyTag interaction. Chem.
1018 Commun. *58*, 13471–13474.

1019 Kuhlman, B., Yang, H.Y., Boice, J.A., Fairman, R., and Raleigh, D.P. (1997). An
1020 exceptionally stable helix from the ribosomal protein L9: Implications for protein folding and
1021 stability. J. Mol. Biol. *270*, 640–647.

1022 Labrijn, A.F., Meesters, J.I., De Goeij, B.E.C.G., Van Den Bremer, E.T.J., Neijssen, J., Van
1023 Kampen, M.D., Strumane, K., Verploegen, S., Kundu, A., Gramer, M.J., et al. (2013).
1024 Efficient generation of stable bispecific IgG1 by controlled Fab-arm exchange. Proc. Natl.
1025 Acad. Sci. U. S. A. *110*, 5145–5150.

1026 Labrijn, A.F., Janmaat, M.L., Reichert, J.M., and Parren, P.W.H.I. (2019). Bispecific
1027 antibodies: a mechanistic review of the pipeline. Nat. Rev. Drug Discov. *18*, 585–608.

1028 Law, S.M. (2020). Modevectors. https://pymolwiki.org/index.php/Modevectors (Accessed 2
1029 February 2022).

1030 Li, X., Pan, C., Sun, P., Peng, Z., Feng, E., Wu, J., Wang, H., and Zhu, L. (2022). Orthogonal
1031 modular biosynthesis of nanoscale conjugate vaccines for vaccination against infection. Nano
1032 Res. *15*, 1645–1653.

1033 Matsunaga, R., Yanaka, S., Nagatoishi, S., and Tsumoto, K. (2013). Hyperthin nanochains
1034 composed of self-polymerizing protein shackles. Nat. Commun. *4*, 2211.

1035 Mineev, K.S., Bocharov, E. V., Pustovalova, Y.E., Bocharova, O. V., Chupin, V. V., and
1036 Arseniev, A.S. (2010). Spatial Structure of the Transmembrane Domain Heterodimer of
1037 ErbB1 and ErbB2 Receptor Tyrosine Kinases. J. Mol. Biol. *400*, 231–243.

1038 Mirdita, M., Schütze, K., Moriwaki, Y., Heo, L., Ovchinnikov, S., and Steinegger, M. (2022).
1039 ColabFold: making protein folding accessible to all. Nat. Methods *19*, 679–682.

1040 Mohan, K., Ueda, G., Kim, A.R., Jude, K.M., Fallas, J.A., Guo, Y., Hafer, M., Miao, Y.,
1041 Saxton, R.A., Piehler, J., et al. (2019). Topological control of cytokine receptor signaling
1042 induces differential effects in hematopoiesis. Science *364*, eaav7532.

1043 Moraga, I., Richter, D., Wilmes, S., Winkelmann, H., Jude, K., Thomas, C., Suhoski, M.M.,
1044 Engleman, E.G., Piehler, J., and Garcia, K.C. (2015). Instructive roles for cytokine-receptor
1045 binding parameters in determining signaling and functional potency. Sci. Signal. *8*, 1–17.

1046 Nielsen, H., Tsirigos, K.D., Brunak, S., and von Heijne, G. (2019). A Brief History of Protein
1047 Sorting Prediction. Protein J. *38*, 200–216.

1048 Oganesyan, V., Peng, L., Bee, J.S., Li, J., Perry, S.R., Comer, F., Xu, L., Cook, K., Senthil,
1049 K., Clarke, L., et al. (2018). Structural insights into the mechanism of action of a biparatopic
1050 anti-HER2 antibody. J. Biol. Chem. *293*, 8439–8448.

1051 Pardee, K., Green, A.A., Ferrante, T., Cameron, D.E., Daleykeyser, A., Yin, P., and Collins,
1052 J.J. (2014). Paper-based synthetic gene networks. Cell *159*, 940–954.

1053 Plagmann, I., Chalaris, A., Kruglov, A.A., Nedospasov, S., Rosenstiel, P., Rose-John, S., and
1054 Scheller, J. (2009). Transglutaminase-catalyzed covalent multimerization of camelidae anti-
1055 human TNF single domain antibodies improves neutralizing activity. J. Biotechnol. *142*,
1056 170–178.

1057 Rahikainen, R., Rijal, P., Tan, T.K., Wu, H.-J., Andersson, A.C., Barrett, J.R., Bowden, T.A.,
1058 Draper, S.J., Townsend, A.R., and Howarth, M. (2021). Overcoming Symmetry Mismatch in
1059 Vaccine Nanoassembly through Spontaneous Amidation. Angew. Chemie *133*, 325–334.

1060 Ruskowitz, E.R., Munoz-Robles, B.G., Strange, A.C., Butcher, C.H., Kurniawan, S., Filteau,
1061 J.R., and DeForest, C.A. (2023). Spatiotemporal functional assembly of split protein pairs
1062 through a light-activated SpyLigation. Nat. Chem. *15*, 694–704.

1063 Salimi, F., Forouzandeh Moghadam, M., and Rajabibazl, M. (2018). Development of a novel
1064 anti-HER2 scFv by ribosome display and in silico evaluation of its 3D structure and
1065 interaction with HER2, alone and after fusion to LAMP2B. Mol. Biol. Rep. *45*, 2247–2256.

1066 Scheer, J.M., Sandoval, W., Elliott, J.M., Shao, L., Luis, E., Lewin-Koh, S.-C., Schaefer, G.,
1067 and Vandlen, R. (2012). Reorienting the Fab Domains of Trastuzumab Results in Potent
1068 HER2 Activators. PLoS One *7*, e51817.

1069 Scholl, S., Beuzeboc, P., and Pouillart, P. (2001). Targeting HER2 in other tumor types. Ann.
1070 Oncol. *12*, S81–S87.

1071 Shaw, A., Lundin, V., Petrova, E., Fördos, F., Benson, E., Al-Amin, A., Herland, A.,
1072 Blokzijl, A., Högberg, B., and Teixeira, A.I. (2014). Spatial control of membrane receptor
1073 function using ligand nanocalipers. Nat. Methods *11*, 841–846.

1074 Siddiqui, S., Cong, W.-N., Daimon, C.M., Martin, B., and Maudsley, S. (2013). BRET
1075 Biosensor Analysis of Receptor Tyrosine Kinase Functionality. Front. Endocrinol.
1076 (Lausanne). *4*, 1–11.

1077 Spiess, C., Merchant, M., Huang, A., Zheng, Z., Yang, N.Y., Peng, J., Ellerman, D., Shatz,
1078 W., Reilly, D., Yansura, D.G., et al. (2013). Bispecific antibodies with natural architecture
1079 produced by co-culture of bacteria expressing two distinct half-antibodies. Nat. Biotechnol.
1080 *31*, 753–758.

1081 Stüber, J.C., Richter, C.P., Bellón, J.S., Schwill, M., König, I., Schuler, B., Piehler, J., and
1082 Plückthun, A. (2021). Apoptosis-inducing anti-HER2 agents operate through
1083 oligomerization-induced receptor immobilization. Commun. Biol. *4*, 762.

1084 Sutherland, A.R., Alam, M.K., and Geyer, C.R. (2019). Post-translational Assembly of
1085 Protein Parts into Complex Devices by Using SpyTag/SpyCatcher Protein Ligase.
1086 ChemBioChem *20*, 319–328.

1087 Szijj, P., and Chudasama, V. (2021). The renaissance of chemically generated bispecific
1088 antibodies. Nat. Rev. Chem. *5*, 78–92.

1089 Veggiani, G., Nakamura, T., Brenner, M.D., Gayet, R. V, Yan, J., Robinson, C. V, and
1090 Howarth, M. (2016). Programmable polyproteams built using twin peptide superglues. Proc.
1091 Natl. Acad. Sci. *113*, 1202–1207.

1092 Verheije, H., Kijanka, M., Henegouwen, P.V.B.E., and Rottier, P. (2013). Bi-specific
1093 adapters. International Patent No. WO2013135655A1.

1094 Vester, S.K., Rahikainen, R., Khairil Anuar, I.N.A., Hills, R.A., Tan, T.K., and Howarth, M.
1095 (2022). SpySwitch enables pH- or heat-responsive capture and release for plug-and-display
1096 nanoassembly. Nat. Commun. *13*, 3714.

1097 Vijayaraghavan, S., Lipfert, L., Chevalier, K., Bushey, B.S., Henley, B., Lenhart, R.,
1098 Sendecki, J., Beqiri, M., Millar, H.J., Packman, K., et al. (2020). Amivantamab (JNJ-
1099 61186372), an Fc enhanced EGFR/cMet bispecific antibody, induces receptor
1100 downmodulation and antitumor activity by monocyte/macrophage trogocytosis. Mol. Cancer
1101 Ther. *19*, 2044–2056.

1102 Wang, F., Liu, Y., Yu, Z., Li, S., Feng, S., Cheng, Y., and Agard, D.A. (2020). General and
1103 robust covalently linked graphene oxide affinity grids for high-resolution cryo-EM. Proc.

Natl. Acad. Sci. U. S. A. *117*, 24269–24273.

Wei, Q., He, S., Qu, J., and Xia, J. (2020). Synthetic Multienzyme Complexes Assembled on Virus-like Particles for Cascade Biosynthesis in Cellulo. Bioconjug. Chem. *31*, 2413–2420.

Wu, W.H., Wei, J., and Zhang, W. Bin (2018). Controlling SpyTag/SpyCatcher Reactivity via Redox-Gated Conformational Restriction. ACS Macro Lett. *7*, 1388–1393.

Yachnin, B.J., Mulligan, V.K., Khare, S.D., and Bailey-Kellogg, C. (2021). MHCEpitopeEnergy, a Flexible Rosetta-Based Biotherapeutic Deimmunization Platform. J. Chem. Inf. Model. *61*, 2368–2382.

Zhang, X., Gureasko, J., Shen, K., Cole, P.A., and Kuriyan, J. (2006). An Allosteric Mechanism for Activation of the Kinase Domain of Epidermal Growth Factor Receptor. Cell *125*, 1137–1149.

Zheng, J., He, W., Li, J., Feng, X., Li, Y., Cheng, B., Zhou, Y., Li, M., Liu, K., Shao, X., et al. (2022). Bifunctional Compounds as Molecular Degraders for Integrin-Facilitated Targeted Protein Degradation. J. Am. Chem. Soc. *144*, 21831–21836.